Pseudotachylyte remanence confirms generation along low-angle normal fault planes

A THESIS
SUBMITTED TO THE FACULTY OF THE GRADUATE SCHOOL
OF THE UNIVERSITY OF MINNESOTA
BY

Benjamin Maxfield Longchamp

IN PARTIAL FULFILLMENT OF THE REQUIREMENTS
FOR THE DEGREE OF
MASTER OF SCIENCE

Joshua M. Feinberg

June, 2019

Acknowledgements

I owe a tremendous amount to everyone in the Institute for Rock Magnetism, but no one more than my advisor Josh Feinberg who took a chance hiring me two years ago and hopefully doesn't regret it. I never imagined finding a grad school advisor who I enjoyed working with as much as I have enjoyed working with Josh. Others in the IRM who have contributed in both tangible and intangible ways to my work are Peat Solheid, who never once blamed me for breaking something in the lab; Andrea Biedermann, who provided hours of support to my project even as she was getting ready to leave the IRM and move out of the country; Dario Bilardello taught me how to use almost everything in the lab the first time, and sometimes also for a second and third time when I needed reminding; Mike Jackson saved me when I input bad data into the database and agreed to be on my committee at the eleventh hour; and last but certainly not least, Kathryn Hobart for knowing everything about everything and being my first point of contact for all inquiries, especially those related to mineralogy.

The Earth Sciences department at-large was fantastically supportive, both financially and as a community. Thank you to all of my grad student peers for making this department such a fun place to work and organizing so many social events. Also thank you to the numerous department staff who work so hard to make graduate students lives easier. In particular, Jen Petrie is always deserving of recognition for everything she does on our behalf and being exceedingly good at her job in general. The patience and expertise of Mark Griffith was also essential to my sample preparation for this project.

Finally, this project relied significantly on the expertise of Laurel Goodwin, whose knowledge of pseudotachylytes, the South Mountains, and low-angle normal faults is second to none. Her collaboration allowed us to extend this project much further than we otherwise would have been able to.

Contents

List of Figures

List of Tables

Chapter 1

Fundamentals of rock magnetism

1.1 Mineral magnetism basics

All solid materials are magnetic, but there are several different classes of magnetism, not all of which produce materials that are conventionally thought of as "magnets". In order from the weakest to the strongest magnetic responses, the three main classes of magnetization are: diamagnetism, paramagnetism, and ferromagnetism.

1.1.1 Diamagnetism

Every solid exhibits a small diamagnetic response to an applied field (Fig. 1.1A). The induced magnetization, **J**, for a solely diamagnetic material is proportional to the strength of the applied field, **H**, and in the antiparallel direction. The linear dependence between **J** and **H** is known as the magnetic susceptibility, χ. In diamagnetic materials, χ is negative and independent of temperature. Induced magnetization returns to zero when the field is removed.

1.1.2 Paramagnetism

In paramagnetic materials, atoms with unpaired electrons in partially filled orbital shells have non-interacting magnetic moments. Vibrations of the crystal lattice randomly orient the magnetic moments, producing a net zero magnetization in the absence of a field **H**. However, with an applied field, the magnetic moments align with **H** and paramagnetic solids acquire a small magnetization, **J**, parallel and linearly proportional to **H** (Fig. 1.1B). The degree of alignment of the magnetization and the applied field depends on the ratio of aligning energy to thermal energy, given by the Langevin Theory, which defines the probability ($P(\theta)$) of an atomic moment (**M**) having angle θ in a field **H**, at a temperature T is

$$P(\theta) \propto \exp(\frac{\mu_0 MH\cos(\theta)}{kT}),$$

where k is the Boltzmann constant, $MH\cos(\theta)$ is the aligning energy and kT is the thermal energy. This equation demonstrates that the alignment of moments with an applied field in a paramagnetic

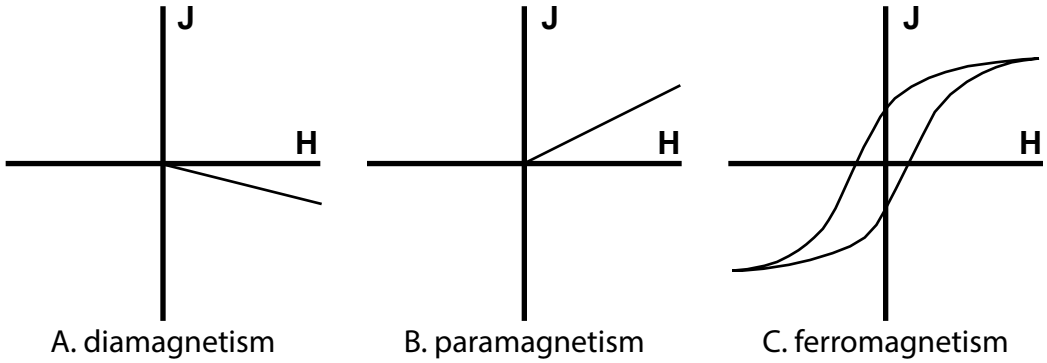

Figure 1.1. Magnetic response (**J**) to applied field (**H**) for (a) diamagnetic materials, (b) paramagnetic materials, and (c) ferromagnetic materials. Adapted from Butler (1992).

material is dependent on temperature, with greater temperatures producing lesser alignment. Increasing temperature energizes the crystal lattice, resulting in more vibrations which increase the randomness of individual magnetic moments and decreases alignment of **J** with **H**.

1.1.3 Ferromagnetism

Like paramagnetic materials, ferromagnetic minerals have atoms with unpaired electrons in partially filled orbital shells. In contrast to paramagnetic materials, atomic moments in ferromagnetic materials interact with one another due to crystal structure. The Pauli exclusion principle states that each electron in an atom must have a unique set of quantum numbers. When atoms with moments are close enough to interact, adjacent atoms must together satisfy the Pauli exclusion principle while having overlapping electron orbitals. This has a coupling effect on adjacent magnetic moments that, unlike diamagnetism or paramagnetism, may persist even in the absence of a magnetizing field. The recorded magnetization is known as remanence, and its direction and strength is related to the field it was acquired in. The relationship between the magnetization, **J**, and magnetizing field, **H**, in ferromagnetic materials varies greatly. Each material has layers of magnetic moments that are coupled (aligned) within the layer, but in the three subcategories of ferromagnetism the coupling between the layers of magnetic moments changes (Fig. 1.2). In a true ferromagnetic material, all the magnetic moments are parallel coupled both within layers and between layers, producing a strong net magnetization. In antiferromagnetic minerals, adjacent layers of moments exactly oppose each other, producing a net zero magnetization. Ferrimagnetic materials also have antiparallel coupling between layers of parallel coupled moments, but the layers of moments are of unequal strength, so there is a non-zero magnetization.

The magnetization of ferromagnetic materials in response to an applied field is nonlinear, and the materials record part of the applied field when it is removed. This type of response is called hysteresis. A hysteresis loop is a bi-plot showing the magnetization of a ferromagnetic sample, **J**, in a magnetic field, **H** (Fig. 1.1C). Important values obtained from a hysteresis loop are saturation magnetization, saturation remanence, coercivity, and coercivity of remanence. Saturation magnetization

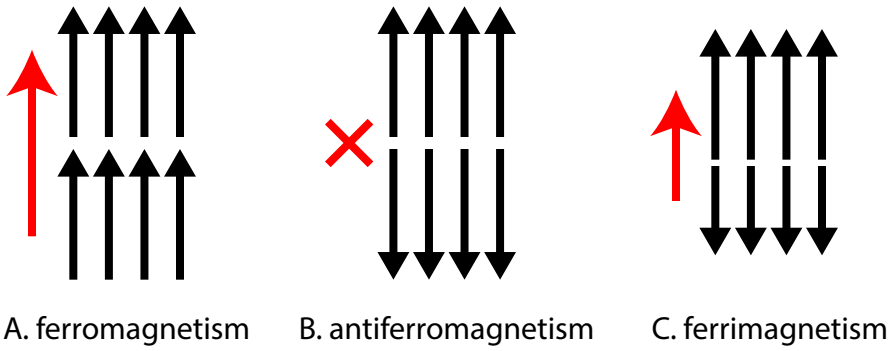

Figure 1.2. The three types of interlayer coupling in a ferromagnetic material. Two layers of moment are shown in black, and the net magnetization is shown in red. (A) true ferromagnetic coupling produces a large net moment, (B) antiferromagnetic coupling produces a net zero moment, (C) ferrimagnetic coupling produces a small net moment. Adapted from Butler (1992).

is the highest magnetization achieved in the presence of a large field. The saturation remanence is the recorded magnetization after a saturating field has been applied and removed. Coercivity is the strength of the magnetizing field applied in the opposite direction which causes the induced magnetization of the sample to be zero. The coercivity of remanence is similar, but is the strength of field that causes the remanent magnetization to be zero when starting with saturation remanence. Hysteresis and back-field measurements are discussed in more detail below.

The degree of alignment between moments and an applied field in a population of single domain ferromagnetic grains is again dependent on the ratio of aligning energy to thermal energy, given by

$$\text{degree of alignment} = \tanh(\frac{vj_s[T_B]H}{kT_B}),$$

where v is the volume of the grain and T_B is the blocking temperature, discussed below. Magnetic response to an applied field of ferromagnetic materials is dependent on temperature. At high temperatures, thermal expansion and vibrational energy decrease coupling between magnetic moments, and at a diagnostic temperature for each mineral, known as the Curie temperature, expansion is such that adjacent moments are no longer coupled and the material behaves paramagnetically (Fig. 1.3).

1.1.4 Single grain scale remanent magnetization

The distribution of magnetic moments within individual grains of ferromagnetic minerals is optimized to minimize the total energy of the grain (Fig. 1.4). Magnetostatic energy resulting from adjacent, like-charges repelling each other is usually the major contributor to the total energy of the grain, and thus the lowest-energy configuration of a grain typically minimizes the magnetostatic energy by reducing the amount of charges on the surface of the grain.

There are two main states that ferromagnetic grains can exist in, based on size. Small grains are known as single domain (SD), and large grains are multi-domain (MD). As the nomenclature implies, the difference between the two types is the presence of two or more magnetic domains. A

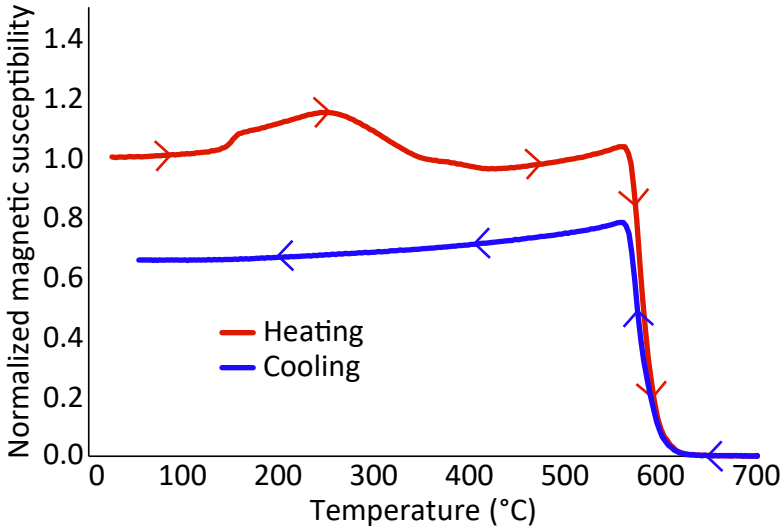

Figure 1.3. Example high temperature susceptibility experiment illustrating the Curie temperature of magnetite at 580°C. Sample is heated from room temperature as susceptibility is measured periodically. After reaching T_C, it is cooled back to room temperature. The sample behaves ferrimagnetically below 580°C and paramagnetically above this temperature.

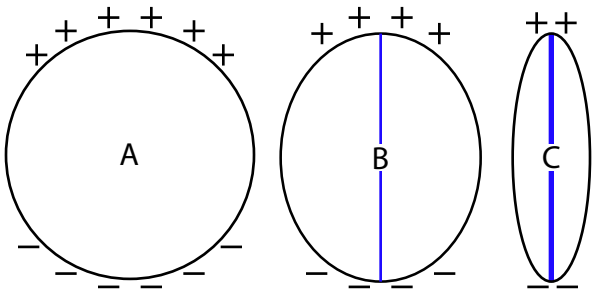

Figure 1.4. Lowest magnetostatic energy configuration of charges for different shape grains. The blue line identifies the magnetostatic easy axis, thicker lines mean higher energy barriers preventing the rotation of the moment away from the easy axis. (A) spherical grain with no shape anisotropy or magnetostatic easy axis, (B) slightly elongate grain with mild shape anisotropy and a magnetostatic easy axis with low energy barriers, (C) elongate grain, with severe shape anisotropy and an easy axis with high energy barriers.

domain is a volume of a grain that is uniformly magnetized such that the magnetization, j, of the domain is equal to its saturation magnetization, $\mathbf{j_s}$. In single domain grains, the entire grain is part of the same domain. Due to the contribution of magnetostatic energy, large grains can reduce their total energy by forming magnetic domains, distinct regions of uniform magnetization within the same grain, separated by domain walls (Fig. 1.5).

In large grains the formation of domains may reduce the magnetostatic energy by separating adjacent like charges and reducing the total number of surface charges, but domain walls take energy to form and maintain so grains cannot be separated into infinitely small domains, but reach a balance point where fewer domains would increase magnetostatic energy, but additional domains would

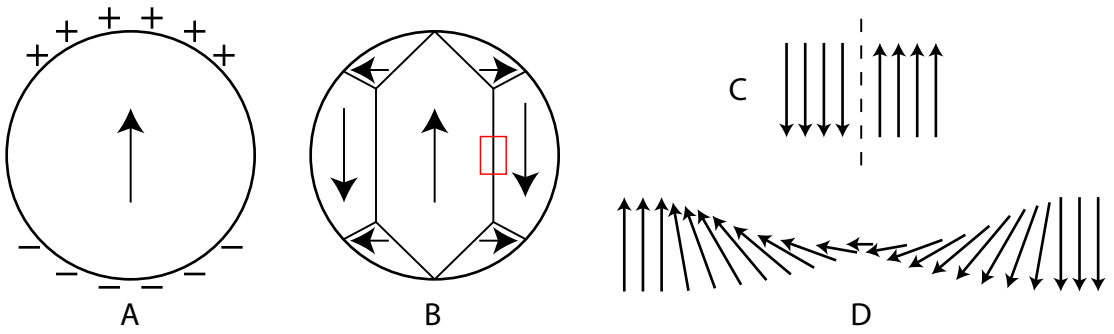

Figure 1.5. (A) Uniformly magnetized spherical SD grain with $\mathbf{j_s}$ given by the arrow and a surface charge distribution shown with + and − symbols. (B) MD grain with $\mathbf{j_s}$ for each domain shown. Red box indicates the domain wall barrier section shown qualitatively in C-D. (C) infinitely thin domain wall, minimizing anisotropy energy but maximizing exchange energy. (D) Infinitely thick domain wall minimizing exchange energy but maximizing anisotropy energy. Figure adapted from Butler (1992) and Moskowitz (1991).

require more energy to form than they would reduce the total energy of the grain. The exchange energy and anisotropy energy determine the width of domain walls. An infinitely thin domain wall minimizes anisotropy energy because all spins are aligned with the easy axis of the crystal, but maximizes exchange energy because adjacent spins directly oppose each other (Fig. 1.5C). An infinitely thick domain wall minimizes exchange energy by keeping adjacent spins parallel, but maximizes anisotropy energy because spins oppose the magnetocrystalline easy axis (Fig. 1.5D). These observations imply domain walls with finite width that minimize total energy of a grain.

Grains with dimensions between stable single-domain and multidomain configurations have historically been referred to as 'pseudosingle-domain grains'. As single-domain grains grow in size, the magnetic moments within the grain begin to curl in a helical fashion to form a magnetic "vortex" state. Recently there has been a move within the rock magnetic community to begin referring to these grains as 'vortex-state' rather than 'pseudo-single domain' grains, since this new name more accurately describes the distribution of magnetization within the grain, whereas 'pseudo-single domain' is more descriptive of the macroscopic behavior (e.g. coercivity and remanence). Vortex state grains can retain magnetizations over geologic timescales, and hence are deeply important to the field of paleomagnetism. In practice, most geological materials are likely to hold a range of grains sizes, extending from superparamagnetic to multidomain. Superparamagnetic grains are smaller than single domain-grains. Small enough grains have zero coercivity and zero remanence at temperatures above 0 K. The result of this is spontaneous magnetization reverals along the easy axis of the grain. Though made of a ferromagnetic material, such grains will behave essentially paramagnetically, but with higher magnetic susceptibility.

Hysteresis is the response a grain has to an applied magnetic field and is different for single-domain and multi-domain grains. In an idealized model of an elongate single domain ferromagnetic grain without an applied field, the direction of magnetization lies along the easy axis, in the minimum energy state, pointing in either direction. An applied field not parallel to the easy axis rotates the magnetization towards the applied field, with stronger fields producing larger rotations, but when

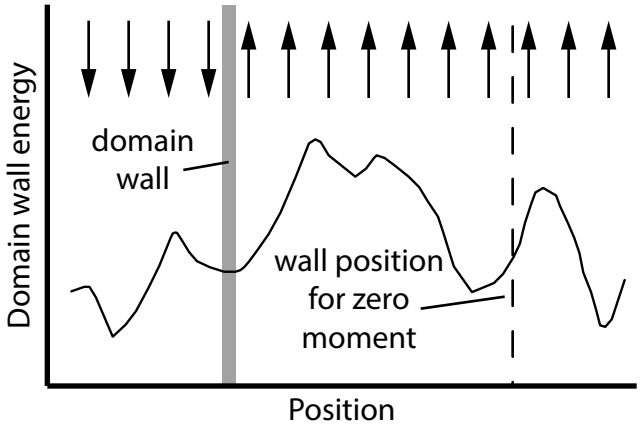

Figure 1.6. Hypothetical example of domain wall energy as a function of position. Walls may settle into a local energy minima, but barriers are low and easily crossed, so MD grain remanence is easily lost to overprint and relaxation. Adapted from Butler (1992).

the field is removed magnetization returns to the easy axis, oriented in whichever direction is closest to the direction before the field was removed. In such an example, the magnetization of the single domain grain is held at high coercivities and stable over time because the magnetization to reverse, it must overcome a large energy barrier to find another energy minima (flipped 180 degrees along the same easy axis).

In multi-domain grains, application of a magnetic field can displace domain walls partially or entirely, and a strong enough field will saturate the grain with a single domain in the direction of the applied field. When such a field is removed, domain walls reform, but may not return to their initial positions (Fig. 1.6). Domain wall energy is a function of position, sensitive to the makeup of each individual crystal; as walls reform they may lie in local minima energy states and retain remanent magnetizations. However, energy barriers holding domain walls in place are small and walls can move easily. Because of this, MD grains tend to have lower coercivities than SD grains and their remanent magnetizations decay with time.

Two major types of anisotropy can affect the recording direction of a single grain: shape anisotropy and magnetocrystalline anisotropy. To understand shape anisotropy, one must be familiar with the internal demagnetizing field: a magnetic field within ferromagnetic grains that directly opposes the magnetization of the grain given by

$$\mathbf{H_D} = -N_D \mathbf{j},$$

where N_D, the internal demagnetizing factor, relates the strength of $\mathbf{H_D}$ to $\mathbf{j}$ and is proportional to the charge density on the grain surface. Magnetostatic energy, e_m, is given by

$$e_m = \frac{N_D j_s^2}{2},$$

so a grain with greater N_D will have greater magnetostatic energy. Shape anisotropy is the tendency

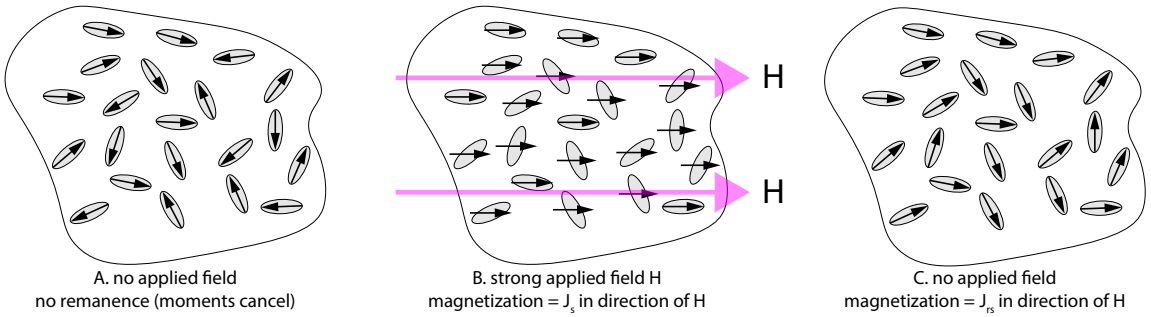

Figure 1.7. Example of remanence acquisition by exposure to a strong magnetizing field. (A) Ferromagnetic grains in a diamagnetic matrix. Sample has net zero magnetization because grains are randomly oriented within the sample and moments are randomly oriented along the easy axis of each grain. (B) In the presence of a strong enough magnetizing field, the moments of each grain rotate parallel with the field, regardless of the easy axis of the grain. The rock reaches saturation magnetization. (C) After saturation, magnetic moments rotate to the closest easy axes to the applied field H. The sample records a saturation remanent magnetization. Adapted from Butler (1992).

of grains to be magnetized along directions that minimize the total surface area of charge, because large surface areas of charge result in high internal demagnetizing factors and higher magnetostatic energy. Directions with the lowest energy are known as "easy" directions, and directions with the hardest energy are "hard" directions.

In grains with very low magnetostatic energy, either due to a lack of shape anisotropy or very low $\mathbf{j_s}$, magnetocrystalline energy can cause anisotropy effects. Different crystallographic orientations can have different energies associated with magnetization along them. Though in magnetite these effects are usually much smaller than shape anisotropy effects, magnetocrystalline easy and hard directions can affect the recording directions in samples as well.

1.1.5 Sample-scale magnetization

When we measure a natural sample, we are not just measuring one ferromagnetic grain, we are measuring the combined magnetization of countless ferromagnetic grains emplaced within a diamagnetic and paramagnetic matrix. Remanence directions we measure are a statistical average of the magnetic vectors of all the ferromagnetic grains in the sample. Consider a dominantly diamagnetic sample with a small percentage of elongate magnetite grains randomly oriented in space with random magnetization directions interspersed. The magnetization we can measure from this rock is zero, since the random magnetizations sum to zero. However, if we apply a strong field, the moment of each ferromagnetic grain aligns with the field direction, as discussed in the single grain magnetization section. Upon removal of the field, moments will align with the easy direction in each grain closest to the applied field direction. The influence of this applied field creates a measurable net magnetization in the direction of the applied field. If the ferromagnetic population of grains was partly or entirely MD grains, the overall magnetization would be weaker and held at lower coercivities, but we would similarly only be able to measure the bulk magnetization of the sample rather than the magnetization of individual grains.

Shape anisotropy is also of concern on a sample-scale. If in the example above the elongate, SD, ferromagnetic grains were not randomly oriented, but all had their easy axes parallel to each other then the magnetization we could measure from the rock would be greatly influenced. After removal of the magnetizing field each grain will return to the lowest energy state along the easy axis. In this manner, preferential orientation of magnetic grains can artificially influence the recording direction measured in a sample. As is discussed below, there are techniques to measure and correct for this type of anisotropy.

1.1.6 Remanence acquisition in nature

The most relevant method to this study by which rocks acquire remanent magnetization is by cooling through the Curie temperature, thereby recording the magnetization of the field the rock was cooled in. Most igneous rocks, including pseudotachylyte, have this type of remanence, known as thermoremanent magnetization (TRM). Though once a grain is cooled below T_c it has a remanent magnetization, the length of time that the magnetization records the field it was acquired in, known as relaxation time, is highly dependent on the temperature (Fig. 1.8). At high temperatures close to T_c, the energy barriers that stabilize remanence are low, so the net magnetization decays very quickly. As the sample cools further below T_C in the same field, the relaxation time increases. The blocking temperature (T_B) of a sample is the temperature at which the relaxation time of the remanent magnetization becomes stable on a time scale relevant to the scientist performing the measurements. Relaxation time changes rapidly with temperature. An SD, elongate magnetite grain may only be stable for 100 seconds at 550° C, but the same grain is stable for billions of years at 510° C.

Rocks sometimes acquire secondary remanence by exposure to a field larger than the coercivity of the ferromagnetic grains it contains. This secondary remanence called isothermal remanent magnetization (IRM) occurs within a few meters of lightning strikes. When exposed to a field stronger than the coercivity of the material, magnetic moments can cross energy barriers holding them in place and flip to alignment along a different easy axis.

1.2 Magnetic characterization techniques

The second half of this chapter focuses on the laboratory techniques relevant to this study. Extensive work has been done to not only measure the demagnetization of our specimens, but to characterize each magnetically in order to best interpret the remanence data.

1.2.1 Demagnetization

At the core of paleomagnetism is the demagnetization of samples to remove any secondary magnetizations and determine the characteristic remanent magnetization (ChRM) directions. Alternating field (AF) demagnetization and thermal demagnetization are the two modern methods that accomplish this. Each relies on progressively inducing magnetic relaxation of the sample in a zero-field environment, starting with the grains that are easiest to relax, usually the largest multi domain or

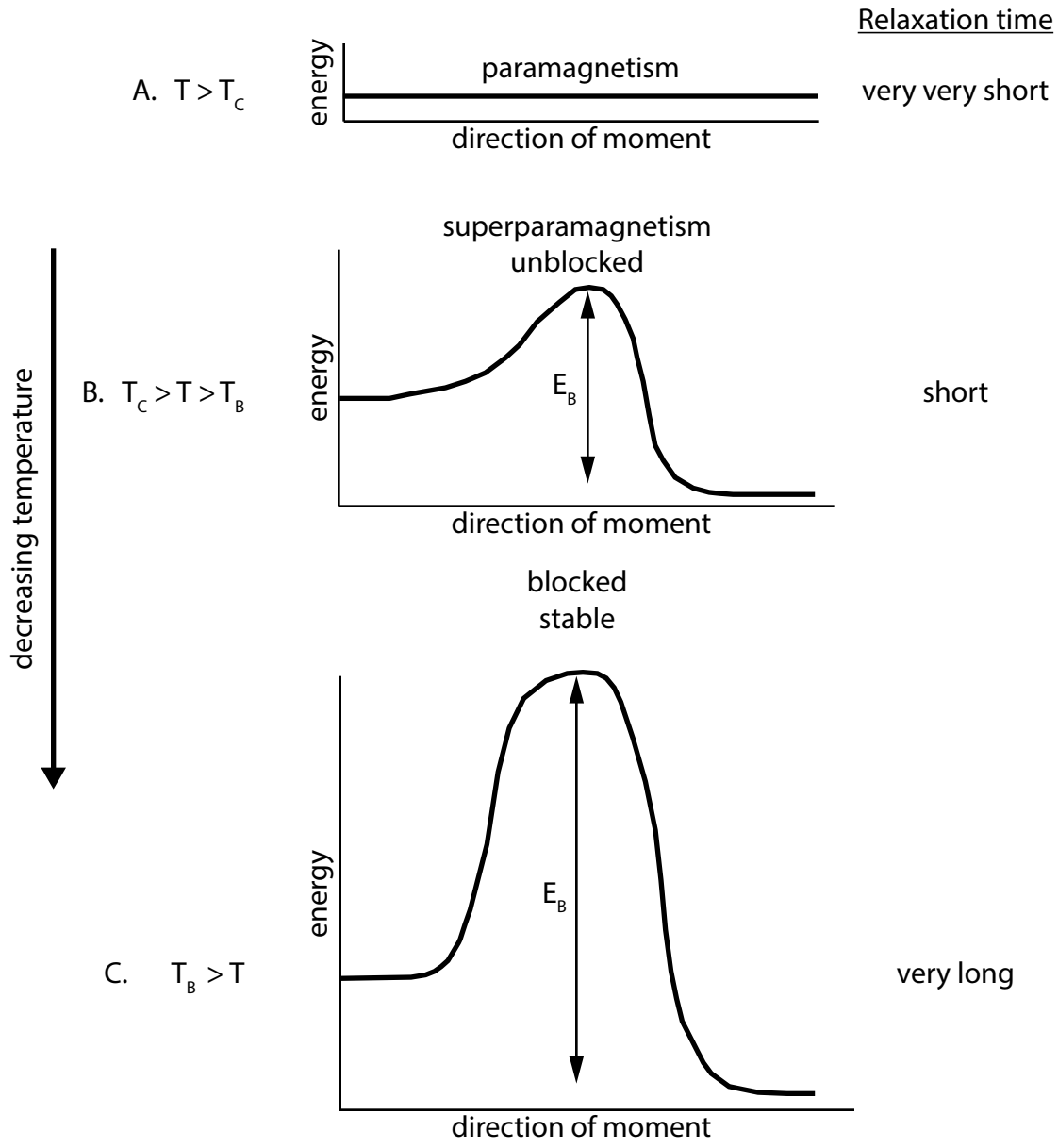

Figure 1.8. Change in energy barriers (E_B) and relaxation time as a ferromagnetic grain cools from above the Curie temperature through the blocking temperature. (A) Above T_C the grain behaves paramagnetically, the moment reflects that of the ambient field and there are no barriers to rotation. (B) Below T_C but above T_B there are small barriers to rotaion. The grain has a remanent magnetization but a short relaxation time. Thermal fluctuations and small changes to the field can easily destroy the recorded magnetization. (C) Below T_B, the energy barriers to rotation become very high. Thermal fluctuations and small fields are no longer enough to decay the remanence on short time scales. Relaxation time is relavent on geologic time scales. Adapted from Moskowitz (1991)

ultrafine viscous super paramagnetic grains, and ending with the grains that are hardest to relax, usually the stable single domain or vortex state grains.

Alternating field (AF) demagnetization

AF demagnetization exposes samples to an oscillating field which is then gradually removed. All moments with coercivities below the peak field strength will track the applied field. As the field is gradually removed, the moments of the individual grains, which all have slightly different coercivities, are locked into a stable orientation in line with one of the two opposing field polarities. The result is a net zero magnetization at coercivities below the peak field, without altering the magnetization of higher coercivity grains. In a single AF demagnetization step, the oscillating field is sequentially applied along each of the X, Y, and Z axes (although not necessarily in that order). In a complete progressive AF demagnetization experiment, this process is repeated several times, increasing the peak-field strength with each iteration and measuring magnetization between each step.

Thermal demagnetization

Thermal demagnetization iteratively heats samples to a steady temperature for a prolonged period of time in a zero-field environment, then cools them back to room temperature, where their magnetization is measured. Similar to AF demagnetization, the initial temperature step is low, and each subsequent step increases until the remaining magnetization in the sample, measured between each step, is reduced to the levels of instrumental noise. This process works to progressively 'erase' magnetizations with lower blocking temperatures because when a grain is heated above T_B, the energy barriers holding the moment in place are easily overcome by thermal fluctuations, and the sample cools back below the blocking temperature, the moments will have a statistical tendency to align with the ambient field. Because this experiment is performed in a magnetically shielded room without an ambient field, the net moment blocked in after each step is zero and the measured magnetization is carried by particles with blocking temperatures above the most recent temperature step.

1.2.2 Demagnetization experiments with laboratory-imparted magnetizations

It is often useful to compare the demagnetization behavior of a natural remanent magnetization of unknown origin to the behavior of a remanent magnetization of known origin produced in a lab. Anhysteretic remanent magnetizations (ARMs) behave broadly similarly to TRMs, and we can produce IRMs in the lab that mimic natural IRMs.

Laboratory ARMs

An ARM is produced by applying two fields to a sample simultaneously: an AF field with a large peak intensity and a DC bias field with a small intensity. The sample is exposed to both fields, and the AF field intensity is reduced to zero while the DC field intensity remains constant.

This acquisition technique is a fast way to replicate the characteristics of a natural TRM because the alternating field has a randomizing effect on the individual moments similar to that of high temperatures, and the bias field can be chosen to be of a similar strength to the Earth's field.

Laboratory IRMs

Laboratory IRM magnetizations replicate natural IRM-inducers like lightning strikes by exposing samples to strong fields for very short durations. Like other laboratory magnetizations they are advantageous because we know the direction of the applied field, whereas lighting strikes tend to randomly orient magnetization directions.

1.2.3 Measuring whole-rock anisotropy

In individual grains, anisotropy creates easy directions of magnetization, directions in the crystal that are lower-energy magnetization states than others, and thus magnetizations preferentially align with those directions. When the easy-axes of single grains are not randomly oriented within a rock the result is anisotropy at the specimen level. Both ferromagnetic and paramagnetic materials may contribute to measureable anisotropy. Anisotropy of ARM measures the anisotropy in remanence-carrying grains using laboratory-imparted ARMs. Anisotropy of magnetic susceptibility measures the anisotropy of the sample in the presence of an applied field, thus capturing the contribution of all mineral grains, weighted according to their specific susceptibilites and abundances.

1.2.4 Anisotropy of remanence

Sample-scale magnetic anisotropy can be calculated using a set of measured laboratory remanences imparted in known orientations. The relationship between the known acquisition fields and the recorded magnetizations can be used to mathematically describe the ferromagnetic fabric in sample. In this study, we calculated the remanence anisotropy based on ARM demagnetizations. Each specimen is repeatedly given an ARM then demagnetized, each ARM magnetization being imparted along a different axis. The process is repeated at least 3 and commonly nine times to obtain sufficient angular coverage. The length of the resulting vector projected onto the acquisition direction from each orientation is called the parallel component. A vector of parallel components for each specimen is multiplied by a matrix of least squares coefficients that is derived from the directions of the applied fields, resulting in a tensor mathematically describing the anisotropy for each specimen. Anisotropy can vary with grain size, so we produced four different AARM tensors per specimen, each measured in a different coercivity window during AF demagnetization. Using matrix algebra, anisotropy-corrected remanence directions can be produced from the measured remanence vectors and anisotropy tensors. The three eigenvector/eigenvalue pairs for each anisotropy tensor describe the principal directions of anisotropy and are used to calculate parameters like degree of anisotropy, ellipsoid shape, lineation, and foliation.

1.2.5 Anisotropy of magnetic susceptibility (AMS)

AMS measures the variation in the magnetization, **J**, of a specimen given the same field, **H**, applied in different orientations. Similar to AARM, the results of an AMS measurement is a tensor describing the three-dimensional relationship between **H** and **J**, with eigenvectors and eigenvalues corresponding to the principal axes of magnetic susceptibility, useful for calculating anisotropy parameters. AMS experiments are advantageous in paleomagnetic studies because they are much faster than AARM and materials with high anisotropy in AMS experiments are more likely to have high anisotropy of remanence. However, AMS measurements cannot be used to quantify or correct for remanence anisotropy because they are measuring the magnetization in the presence of a field, and thus capturing the paramagnetic contribution which does not affect remanence.

1.2.6 Measurement of hysteresis properties

Hysteresis, the ferromagnetic response to an applied field, is measured in this study on a vibrating sample magnetometer (VSM). A VSM vibrates a small volume of sample perpendicular to the field generated by two electromagnets flanking the sample. The change in magnetic flux measured by the instrument is proportional to the magnetic moment of the sample.

The first of two experiments we performed on the VSM estimated saturation magnetization (M_s), saturation remanence (M_{rs}), and coercivity (H_c) by making a hysteresis loop, a series of measurements of magnetization in a systematically varying applied field. An initial large field (usually ≥ 1 T) is applied, then magnetization is recorded as the field is reduced from the maximum value to zero, then increased in the negative direction to the same maximum value, then decreased back to zero and finally increased back to the initial value, creating a loop. M_s is the maximum possible induced magnetization of the sample. Depending on the magnetic mineralogy, the sample may or may not reach saturation. However, magnetite, the only ferromagnetic phase in this study, reaches remanence saturation after exposure to fields greater than 300 mT, so we are finding the true M_rs of our samples. M_{rs} is the remanent magnetization when H has been reduced to 0 after being at saturation, H_c is the applied field strength in the negative direction that reduces M_s to zero. A fourth hysteresis value, coercivity of remanence (H_{cr}) is the applied field strength in the negative direction that reduces M_{rs} to zero.

H_{cr} is measured through the second of two experiments we performed, acquisition of a backfield curve, where a saturated sample is progressively exposed to stronger fields in the negative direction. During this process, magnetization measurements are collected periodically while the field is turned off to capture the remanent rather than induced magnetization.

Hysteresis properties can be diagnostic of certain ferromagnetic minerals, but also provides details about the physical characteristics of the grains. Analysis of backfield curves in this study lead to the breakthrough finding of two distinct grain size populations, which enabled proper interpretation of our remanence measurements.

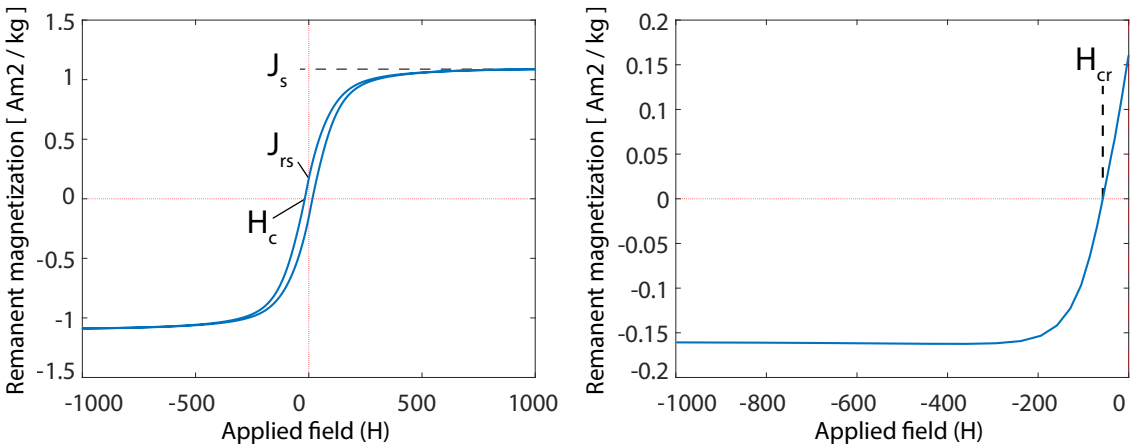

Figure 1.9. Hysteresis loop (A) and backfield curve (B) of a sample measured on a VSM. The sample nears saturation aroud 300 mT indicating magnetite as the primary remanence carrier, and the width of the loop demonstrates that there are remanence carrying grains.

1.2.7 Low temperature characterization

Measuring changes in remanence as a sample is cooled down to or warmed up from very low temperatures offers information about the magnetic mineralogy and grain size population present. The field cooled-zero field cooled (FC-ZFC) experiment compares the magnetization profiles during warming of samples that have cooled from room temperature to 10 K with and without an applied field, and in the latter case, exposed to the same field at 10 K to produce a low-temperature isothermal remanence. Some ferromagnetic minerals have phase transitions that produce noticeable changes in magnetization at diagnostic temperatures that show up in this experiment. For example, the Verwey transition in magnetite around 120 K presents a sharp decrease in remanence on warming, though the exact temperature is sensitive to the individual grain properties. The relative strengths of the FC and ZFC curves also informs about the physical characteristics of the sample. If the FC curve is above ZFC curve it indicates that the magnetization is carried mostly by SD grains, whereas if $M_{ZFC} > M_{FC}$ the magnetization resides in MD grains.

Room temperature saturation IRM (RTSIRM) low temperature demagnetization experiments show similar features as FC-ZFC curves. Samples are given a strong IRM at room temperature, then measured while cooling in zero field to 10 K, and subsequent reheating to room temperature. During the cooling and heating phases, transitions like the Verwey that affect the strength of remanence can be seen. SD grains are more resistant to low-temperature demagnetization than MD grains, so the difference in strength between the initial SIRM and the final magnetization reflects the contributions of SD vs MD grains to the overall magnetization, where a greater difference indicates more MD grains.

1.3 High temperature magnetic susceptibility

Magnetic susceptibility changes as a function of temperature due to the physical properties of minerals and alteration that can occur as a result of heating. A simple experiment measuring the magnetic susceptibility of a powdered sample as it's heated is useful for magnetic mineral identification based on diagnostic Curie temperatures, which results in sharp decreases in susceptibility (Fig. 1.3).

Chapter 2

Paleomagnetism study of pseudotachylytes from low-angle normal faults in the South Mountains, AZ

2.1 Introduction

Pseudotachylytes are the fossil records of ancient earthquakes (Zechmeister et al., 2007, Ferre et al., 2012), where during large rupture events enough energy is released as heat to melt the rock along the fault surface. This melt quenches almost instantaneously into dark pseudotachylyte veins composed partly of ultra-fine grained minerals that nucleated in the melt and partly of larger grains that originated in the host rock and survived the melting event. Pseudotachylyte is unique in the rock record because it is formed contemporaneously with fault rupture. Thus, it may provide a window into conditions at the precise time of seismicity.

Sibson (1975) describes the origin and mineralogic characteristics of pseudotachylytes in great detail. Primary or "generation" veins are largely planar and occur along the fault slip surface (Fig. 2.1). Subsidiary "injection veins" may form oblique to the generation vein as the melt is forced into fractures created during brittle deformation.

Pseudotachylytes offer the geomagnetic community a chance to recover recordings of the Earth's magnetic field at the time of rupture. For veins in the South Mountains of Arizona, Goodwin (1999) reports that the melt forms and quenches within seconds to minutes after rupture. Even if ferromagnetic phases are absent in the host rock, magnetite will crystallize within the pseudotachylyte vein as long as the host contains common iron-bearing minerals (eg. biotite, hornblende) (Ferré et al., 2005). In the South Mountains, it has been shown that psedotachylyte melt and immediately adjacent host rock is super-heated to temperatures above 1000°C, which is sufficiently high to remagnetize any ferromagnetic material in the pseudotachylyte. (Goodwin, 1999).

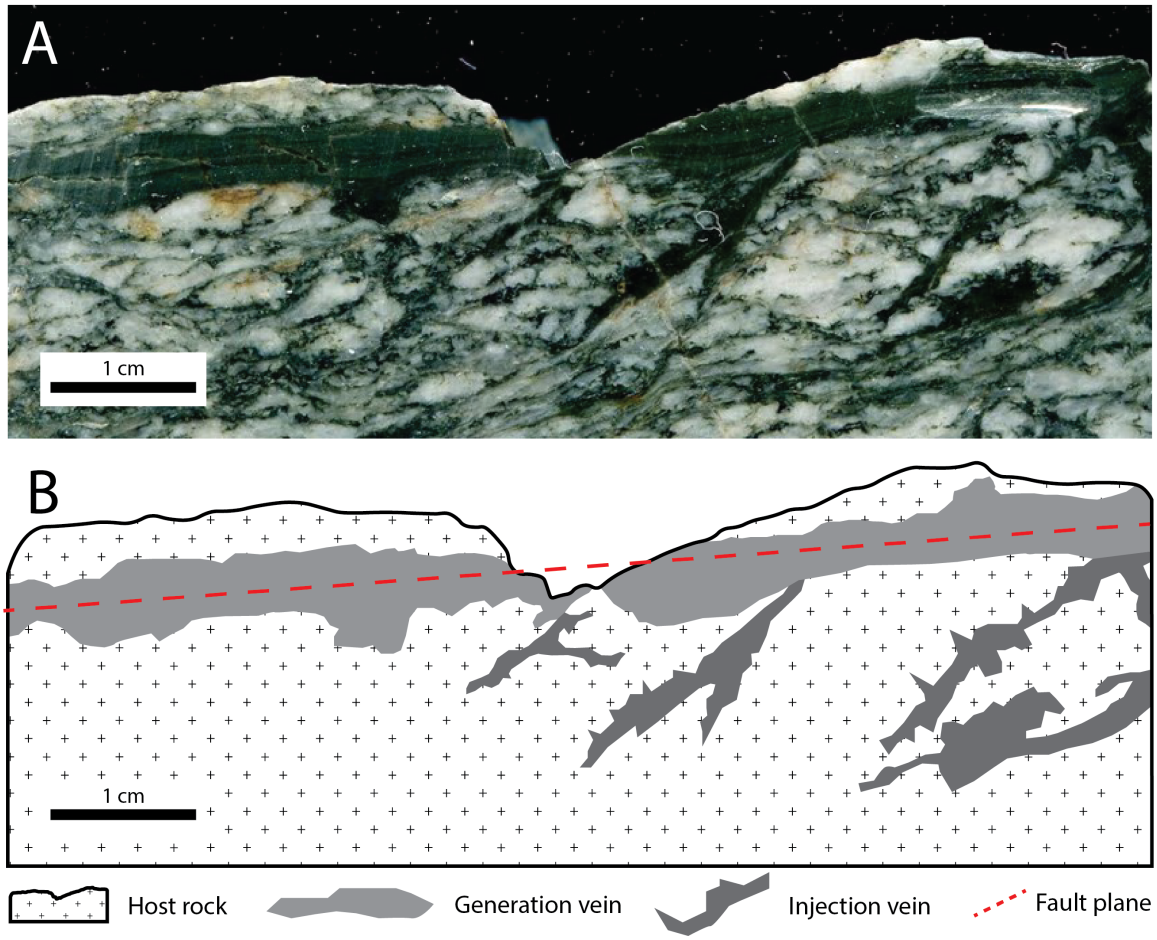

Figure 2.1. Structure of pseudotachylyte in hand sample from the South Mountains. The generation vein lies along the fault plane, while thinner injection veins may be oriented at high angles to the generation vein. Image in (A) courtesy of Jack Hoehn.

Though pseudotachylytes have been well characterized, structurally and magnetically, it is rare to find an instance where paleomagnetic directions are recovered and applied to a larger scale problem. In this study, we attempt to use the remanence directions of pseudotachylyte from the South Mountains metamorphic core complex of Arizona to contribute to the ongoing debate about the origin of low-angle normal faults.

2.1.1 Review of structural debate surrounding low-angle normal faults

Normal faults, following the mechanical model outlined by Anderson (1951), are optimally oriented when they dip $\approx 60^\circ$ from horizontal. Anisotropies in the crust allow normal faults to be oriented at shallower angles, but some research suggests that normal faults should not produce earthquakes shallower than 30° (Jackson and White, 1989, Collettini and Sibson, 2001). Presently, pseudotachylyte veins along normal faults in the South Mountains dip on average 18°, but the angle at which the faults failed seismically remains an active research question (Smith, 2013). Indeed,

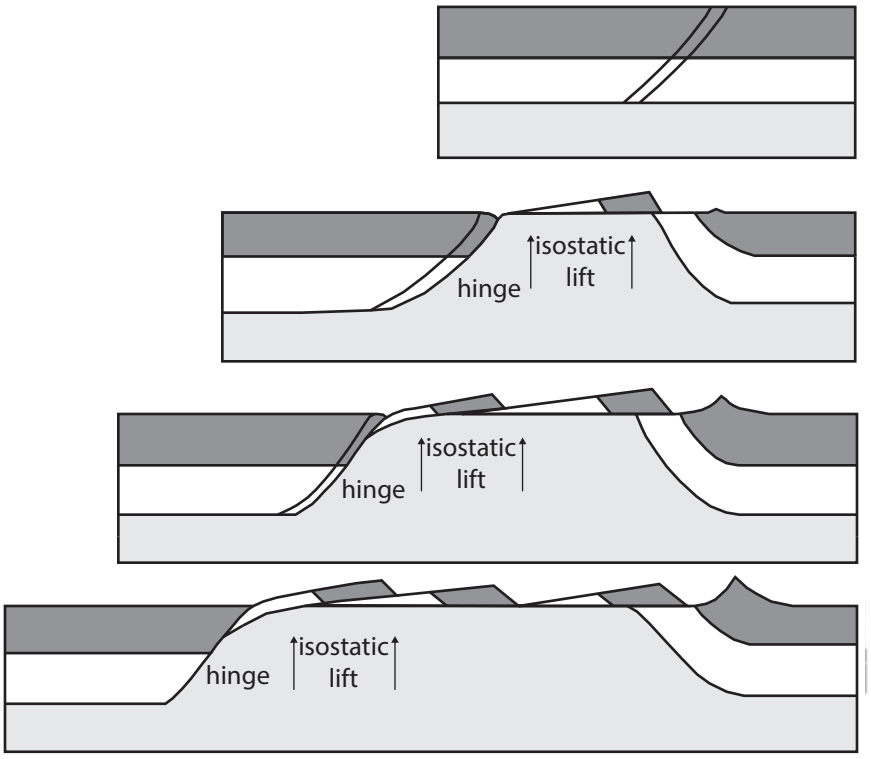

Figure 2.2. The rolling hinge model predicts steeply dipping normal faults that rotate to shallow dips via isostatic uplift during exhumation. At a threshold dip, around 30°, continued extension along the same fault plane becomes unfavorable and new, steep faults form. Adapted from Wernicke (1992).

for most core complexes in the North American Cordillera there is open debate about the initial orientation of normal faults that today appear to be low-angle.

The rolling hinge model (Fig. 2.2) has garnered attention as a potential solution that does not require seismicity along low-angle normal faults (Spencer, 1984, Buck, 1988, Wernicke and Axen, 1988). There is a conclusive body of paleomagnetic evidence to support the rolling hinge model in oceanic core complex settings (reviewed at length in Whitney et al. (2013)), but it is unclear if the same mechanisms are responsible for low-angle normal faults in continental settings such as the South Mountains. According to the rolling hinge model, normal faults originate in orientations favored by classic fault mechanical theory (Anderson, 1951) (30° from the maximum principal stress direction, $\approx 60°$ from horizontal). As extension continues along the fault, isostatic rebound in the crust rotates the fault to shallower dips. At some threshold dip, the fault is abandoned because it becomes mechanically favorable to initiate a new fault at a steeper dip. Over time, this model creates a system of apparently low-angle normal faults that were seismically active only at steeper angles.

There is significant uncertainty over the applicability of rolling-hinge models to many terrestrial field sites. Analytical studies have concluded that large-magnitude seismicity along low angle normal

faults is mechanically unfavorable (Wills and Buck, 1997), and there is field data to support the idea that earthquakes do not occur on low angle normal faults (Jackson, 1987, Jackson and White, 1989), though they do allow for aseismic creep (Collettini et al., 2009). In contrast to these findings, some workers in the field do report evidence for seismicity on low-angle normal faults (John and Foster, 1993, Monigle et al., 2012). Field relationships in some areas indicate that many low angle normal faults can initiate through time by, demonstrated by low-angle structures both cutting and being cut by high angle structures in the same locality (Davis and Lister, 1988, Scott and Lister, 1992, John and Foster, 1993). Paleomagnetic work on footwall rocks (not pseudotachylytes) from our field area have also indicated a low amount of overall regional tilting, which is interpreted as support for slip along low-angle structures because faults would have been active near their present orientations (Livaccari et al., 1995). Lubricating minerals along fault planes have been suggested as a mechanism that could allow for low-angle slip (Monigle et al., 2012), but others qualify that this could only happen due to clay gouge along reactivated fault planes that had initiated at high angles (Haines et al., 2014).

The purpose of this study is to use the remanence direction of pseudotachylyte veins, unambiguous markers of both paleo-fault planes and paleo-seismicity, to test the orientation of the fault at the time of rupture and thereby contribute to the ongoing debate on the origin of low-angle normal faults. I have demagnetized all pseudotachylyte samples collected from low-angle normal faults in the South Mountains metamorphic core complex, incorporated high spatial resolution ultraviolet laser ablation microprobe (UVLAMP) $^{40}Ar/^{39}Ar$ ages (Hoehn et al., 2018), and interpreted the microstructure of several representitive veins. Considerable effort has been put forth to determine the quality of remanence recorded, including correcting for remanence anisotropy and isolating the coercivity profiles of new magnetite grains that nucleated in the pseudotachylyte melt. In the following chapter I present a strong body of evidence to support pseudotachylyte generation along low-angle normal faults.

2.2 Geologic setting of the South Mountains

The South Mountains Metamorphic core complex near Phoenix, AZ is part of a belt of core complexes extending from Mexico through the western United States and into Canada. Extension in the South Mountains began ca. 22 Ma and continued until at least 16.5 Ma along a northeast-southwest trending detachment fault (Reynolds et al., 1986). This study is focused on rocks from the northeast portion of the South Mountains, where there is a dominantly granodiorite lithology, mylonitized to varying degrees (Reynolds et al., 1986).

The mylonitized granodiorite rock is host to an abundance of pseudotachylyte veins. Those exposed at our field site (33.3747 N, 111.9825 W) dip on average 14° to the northeast (Smith, 2013). Veins are thin ($\leq$ 1 cm) and contain varying amounts of inherited host rock clasts. In cross section veins appear planar, but may have more complex geometries in three dimensions. The pseudotachylyte veins themselves are foliated and show preferential orientation of elongate grains. For a complete description of the veins microstructure readers are referred to Smith (2013).

Table 2.1. Summary of thermochronology from the South Mountains granodiorite.

Temperature (°C)	Age (Ma)	1σ Error (Ma)	Method	Source
Whole rock max age	24.9	3.0	Rb-Sr (whole rock)	Reynolds et al. (1986)
800	22.0	4.1	U-Th-Pb (zircon)	Reynolds et al. (1986)
550	20.7	0.4	$^{40}Ar/^{39}Ar$ (hornblende)	Fitzgerald et al. (1993)
250	20.2	0.4	$^{40}Ar/^{39}Ar$ (biotite)	Reynolds et al. (1986)
125	17.5	1.0	apatite fission track	Fitzgerald et al. (1993)
PST rupture NE-106	17.41	0.18	$^{40}Ar/^{39}Ar$ (PST vein)	Smith (2013)
PST rupture NE-103	16.15	0.09	$^{40}Ar/^{39}Ar$ (PST vein)	Smith (2013)

2.2.1 Thermochronology

It is important that the age of the host rock is known so that we may establish a reference direction to compare our results against; thermochronology for the host South Mountains granodiorite pluton in the South Mountains is reasonably well constrained. Reynolds et al. (1986) report a maximum age of 24.9 ± 3.0 Ma from Rb-Sr whole-rock dating and finds the emplacement age (800°)C to be 22 ± 4.1 Ma using U-Pb dating of zircons within the granodiorite. $^{40}Ar/^{39}Ar$ ages from horneblende and biotite, respectively, in the granodiorite record rapid cooling to 550°C by 20.7 ± 0.4 Ma (Fitzgerald et al., 1993) and 300°C by 20.2 ± 0.4 Ma (Reynolds et al., 1986). Apatite fission track data with a closure temperature at 125°C give 17.5 ± 1.0 Ma. Fitzgerald et al. (1993) interpreted the most recent limit of 17.5 Ma as indicating the end of unroofing and seismicity. Smith (2013) finds $^{40}Ar/^{39}Ar$ ages from pseudotachylyte veins as young as 16.2 ± 0.2 Ma, which is essentially the same within error, implying that seismicity continued until at least about 16.5 Ma. These results are summarized in Table 2.1.

2.2.2 Reference direction

We calculate our reference direction (352°, 51°) from the apparent polar wander path of Besse and Courtillot (2002), while acknowledging that pseudotachylyte veins were forming over a period in excess of a million years (Fig. 2.3). We are certain that the earliest time veins could have formed is about 20.2 ± 0.4 Ma based on crosscutting of greenschist facies, and we know that vein formation persisted until at least 16 Ma. Our reference direction was chosen to reflect the time frame within which most pseudotachylyte formed. Though we have plotted our reference direction to reflect the most-likely time of formation (20-16.5 Ma), we also show that the field direction has not changed dramatically from then until the present day, so even though the dates of formation are not precise for all samples, we are still comparing mean directions to acceptable approximations of the reference direction. Further, because pseudotachylyte veins cool rapidly to host rock temperature, which in this time frame is far below the curie temperatures for magnetic phases, the recorded magnetization will capture the effects of secular variation. The reference direction obtained from the age of the veins is time averaged, so we impose a 15° error window to account for secular variation effects in pseudotachylyte (McElhinny and McFadden, 1997).

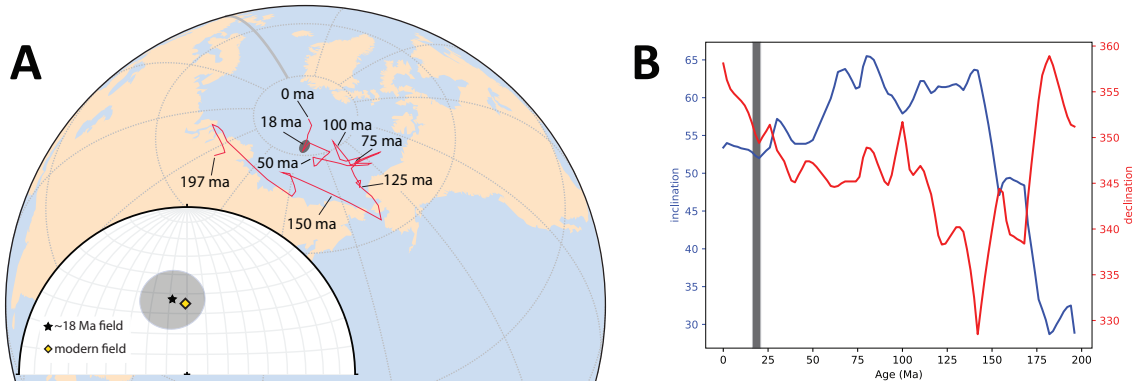

Figure 2.3. (A) Apparent polar wander path for a fixed North America over the last 200 million years. Dark grey ellipse around 18 ma mark denotes most likely period of pseudotachylyte formation in the South Mountains. Latitudes shown are 80°N, 60°N, and 30°N; longitude is shown in 30° increments from the prime meridian, denoted by solid grey line. Inset equal area net shows reference direction for South Mountains site during period of pseudotachylyte formation with error ellipse equal to the extent of expected secular variation at the site latitude based on Model G of McFadden et al. (1988). The yellow diamond indicates the modern field direction, which has changed very little in the past 20 Ma. (B) Inclination and declination changes over the past 200 million years for the Northeast site. Grey shaded region is the period during which pseudotachylyte in the South Mountains was forming from 20 Ma to 16.5 Ma. Apparent polar wander data from Besse and Courtillot (2002), paths calculated using programs adapted from PmagPy toolkit (Tauxe et al., 2016).

2.3 Methods

2.3.1 Sample preparation

Hand samples of pseudotachylyte veins and adjacent host rock were oriented and collected in the field by collaborator Jack Hoehn. Between three and five cores 1 cm in diameter were drilled, each containing pseudotachylyte and host rock. The pseudotachylyte veins were trimmed out of the cores using a wafering saw with a non-magnetic blade. Orientation was maintained throughout processing. A small number of unoriented specimens were collected from various hand samples for magnetic characterization. These specimens were cut to be as close to pure pseudotachylyte vein or pure host rock as possible. Most drill cores labeled as pseudotachylyte or host contain minor amounts of the other type.

2.3.2 Demagnetization experiments

Trimmed samples of pseudotachylyte and host rock were demagnetized in the magnetically shielded room at the Institute for Rock Magnetism at the University of Minnesota, which has a background field of <500 nT. Alternating field (AF) demagnetization was performed along three axes in a 2G superconducting rock magnetometer (SRM), equipped with a U-Channel track system sample handler and an inline 3-axis degausser. Eight specimens were demagnetized at a time, the degauss velocity was 15 cm/s, background velocity 5 cm/s, load velocity 5 cm/s, and sensor velocity

10 cm/s. Progressive demagnetization used fields of (all units mT) 0, 1, 2, 3, 4, 5, 8, 10, 13, 15, 20, 25, 30, 35, 40, 45, 50, 60, 70, 80, 100, 120, 140, 160, and 170.

Thermal demagnetization began with a measurement of each specimen at room temperature. Then, we heated each specimen from 100°C to 650°C in 50°C increments. The specimens were heated together in air and were held at-temperature for a minimum of 40 minutes, before being allowed to cool back to room temperature prior to measuring. Magnetizations were measured at each increment step using a 2G cryogenic rock magnetometer with a manual sample handler.

Anhysteretic remanent magnetizations (ARMs) were imparted using the in-line ARM subsystem on the 2G U-channel SRM at the Institute for Rock Magnetism. Specimens were first demagnetized in a 170 mT field, then given an axial ARM in a 50 μT bias field with a 110 mT AF along the +Z axis. The specimens were then demagnetized according to the same AF-demagnetization procedure outlined above.

We also imparted isothermal remanent magnetizations (IRMs) to all of our samples, then demagnetized them in a manner consistent with our AF-demagnetization of NRM and ARM. To impart the IRMs, we first demagnetized each specimen to 170 mT, then gave each a 60 mT IRM along the Z axis three times consecutively. The sample velocity during demagnetization was decreased for certain samples to as low as 3 cm/s to control for instrumental drift when measuring more strongly magnetized samples.

2.3.3 Anisotropy of Magnetic Susceptibility (AMS)

Anisotropy of magnetic susceptibility was measured at room temperature in a MFK1-FA Kappabridge operated with a field of 200 A/m and a frequency of 976 Hz. Second rank tensors were fit to susceptibility data collected with an automated rotation system.

2.3.4 Anisotropy of anhysteretic remanent magnetization (AARM)

We used AARM to measure and correct for the remanence anisotropy in our samples, following the work of Biedermann et al. (2019). We imparted ARM magnetizations in nine different specimen orientations, using the same method as previously used for ARM, then demagnetized them in a consistent orientation using the same procedure as our NRM, except only using four demagnetization steps: 0 mT, 15 mT, 30 mT, 70 mT, and 170 mT. These steps were chosen qualitatively based on where we commonly saw directional changes during previous AF demagnetization experiments. ARMs were imparted in nine orientations: X, Y, Z, XY, -XY, XZ, -XZ, YZ, -YZ. While acquisition directions were systematically varied, demagnetization always occurred with the samples in the '+Z' orientation with respect to the instrument using three orthogonal AF coils. AARM tensors, calculated from the surviving remanence after each of the AF steps, were used to determine shape and degree of anisotropy for each specimen in each coercivity window, calculate angular and intensity deviation, and correct the NRM data.

2.3.5 Hysteresis properties

Hysteresis loops, backfield curves, and first-order reversal curves (FORCs) were measured at room temperature on a Princeton Measurements Model 3900 "MicroMag" vibrating sample magnetometer. Hysteresis loops were measured with a maximum field of 1 T, at increments of 5 mT, and averaging between 100 ms and 200 ms depending on the strength of the sample. Backfield curves were measured with 50 points from 10 μT to 1 T, with an averaging time between 1 second and 2 seconds, depending on the strength of the sample.

2.3.6 Electron microprobe

Electron microprobe images along with energy-dispersive spectrometry (EDS) and wavelength-dispersive spectrometry (WDS) compositional spectra were collected on the JEOL JXA-8530F Plus microprobe at the University of Minnesota. EDS images and analyses were collected using Pathfinder software and a Thermo ultraDry SDD 10 mm^2 detector, EDS maps used a 10 kV accelerating voltage and either a 10 nA or 40 nA focus beam current. We collected two WDS maps. One large map used a 10 kV accelerating voltage, 100 nA focus beam current, and an 8 ms dwell time on a pixel size of 1 μm. Four WDS detectors were used, LIFL, PETL, TAPL, and PETJ, detecting Fe, Ti, Si, and K, respectively. A smaller WDS map of a magnetite grain was collected using a 10 kV accelerating voltage, 10 nA focused beam current and 130 ms dwell time on a 0.1 μm pixel size. The detecting elements were the same as for the first map, except analyzing for O on LDE1 instead of K on PETJ.

2.4 Results

2.4.1 Electron Microprobe

Images, EDS, and WDS spectra of polished, carbon coated thin sections were taken using an electron microprobe. We specifically targeted oxides within the host and pseudotachylyte to determine compositional and microstructural differences that could help differentiate between relict and neo-formed iron oxides within the pseudotachylyte veins. We also used EDS and WDS spectra to investigate compositional differences between grains and within single large grains.

Found only in the pseudotachylyte veins, euhedral iron-oxide grains 2 μm to 5 μm in size with homogeneous interiors are interpretted as neo-formed magnetite (Fig. 2.4A,B). The composition of neo-formed grains was around 43% iron and 57% oxygen by number of atoms, consistent with the composition of magnetite (Fe_3O_4). Such grains are typically found with their long axis parallel to the fabric of the pseudotachylyte vein (Fig. 2.4A), and sometimes formed in a line with other grains along that fabric (Fig. 2.4E). Iron oxide grains in the host rock are significantly larger, tens of μm across instead of just a few μm, and are fractured near the edges (Fig. 2.4C). The interiors of these grains have three orientations of linear zones that are lower in iron than the surrounding material (Fig. 2.5). These features resemble Ti-lamellae within magnetite, but there is no evidence for Ti within the large magnetite grains, in lamellae or otherwise. Additionally, some grains of magnetite in the host rock are found near or surrounding small zircon grains.

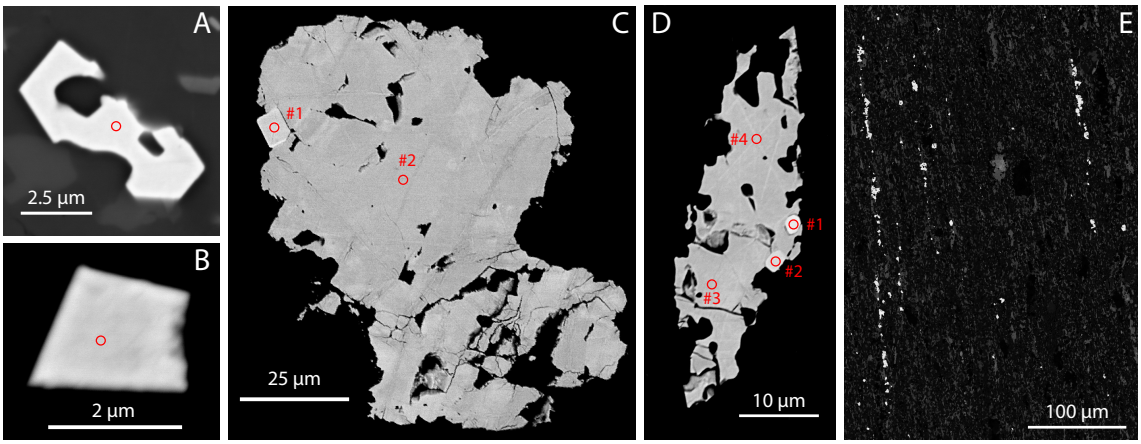

Figure 2.4. Backscattered electron micrographs of oxide grains in pseudotachylyte and host rock. Red circles are location of EDS compositional measurements, reported in Table 2.2. (A) neo-formed magnetite grain within the pseudotachylyte in sample NE-212. The long axis of the grain is parallel to the mineral fabric in the pseudotachylyte vein. (B) Neo-formed magnetite grain within pseudotachylyte in sample NE-6 15-4 XZ. (C) Large magnetite grain from host region of sample AZ UW 12 MI-4 YZ containing a euhedral zircon grain (upper left). The interior of the grain is heterogenous, with both fractures and linear features resembling lamellae. (D) Relict host magnetite grain found within the pseudotachylyte vein in sample NE-6 15-4 XZ. The grain is fractured and has linear, lamellae-like features. There are two zircon inclusions in the grain, and the long axis is again parallel to the pseudotachylyte fabric. (E) Foliation defined by mineralogical domains (subvertical in this image) within pseudotachylyte AZ UW 12 MI-4 XZ. Both neo-formed and relict magnetite grains align in chains parallel to the fabric in the rock. This is a reason to suspect that there may be significant anisotropy in the magnetic properties of the specimen.

The differences between those types of grains allow us to identify large magnetite crystals currently included in the pseudotachylyte which formed in the host rock, prior to pseudotachylyte formation. These grains are much larger than the neo-formed grains, contain linear zones or alteration within them, and may still be associated with zircon grains. These usually anhedral grains may have their long axis oriented parallel to foliation in pseudotachylyte, which I interpret these grains as survivor clasts (i.e., they survived melting in pseudotachylyte) (Fig. 2.4D).

2.4.2 Hysteresis data

We measured 25 hysteresis loops (Fig. 2.6), backfield curves, and first-order reversal curves (FORCs) on 24 specimens, 11 pseudotachylyte and 13 host rock, repeating the measurement on one specimen in a different orientation to investigate anisotropy. Of the 24 specimens, 11 (6 pseudotachylyte, 5 host) were the specimens that this study primarily focused on. These are oriented cores for which we also collected NRM demagnetization data, ARM, AARM, and AMS data. The remaining 13 specimens were collected from the same hand samples as our oriented cores, but are small chips intended be either entirely pseudotachylyte or entirely host material. This is in contrast to the oriented cores, which inevitably contain at least small percentages of both materials.

Host rocks had significantly lower coercivities (Bc) and coercivities of remanence (Bcr) than their

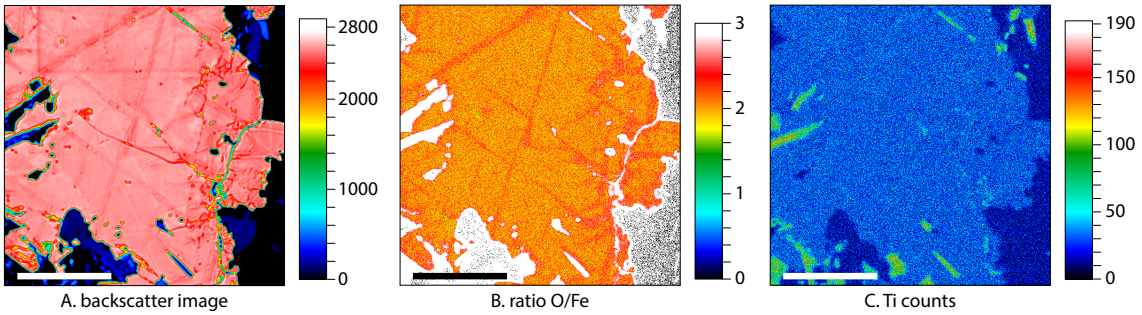

Figure 2.5. Selected results from WDS maps exploring lamellae features on magnetite grain in host rock. Scale bar in lower left of each image is 20 microns. Color bars are based on count data using a 10 kV accelerating voltage, 10 nA focus beam current and 130 ms dwell time on a 0.1μm pixel size. (A) Backscatter image of large host magnetite grain (pink), lamellae appear as darker pink, linear features. (B) Pixels are shaded by Oxygen/Iron ratio. Lamellae features have higher O/Fe than the bulk grain. (C) Pixels shaded by Ti concentration. Magnetite crystal has essentially no Ti, and the lamellae are no longer visible. Small grains rich in both Ti and O are unrelated to the magnetite grain.

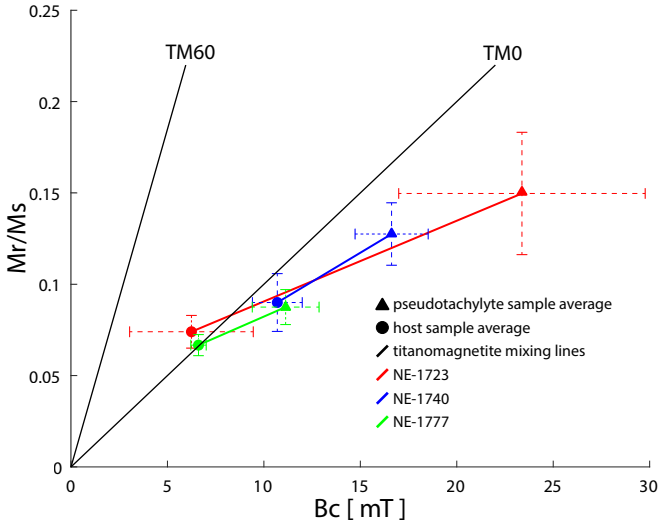

Figure 2.6. Average hysteresis properties of hand samples. Pseudotachylyte specimens had consistently higher coercivities and Mr/Ms ratios than their associated host specimens, attributed to small, neo-formed magnetite grains within the pseudotachylyte matrix. Errors are 1σ. Compositional trend lines are from Wang and Van der Voo (2004). TM60 represents the expected trend for magnetite with 60% Ti-substitution, whereas TM0 rmpresents magnetite with no Ti-substitution.

associated pseudotachylyte (Fig. 2.6). Most pseudotachylytes had Bc $>$ 12 and Bcr$>$ 45, while most hosts had Bc $<$ 12 and Bcr$<$ 36. Further, most pseudotachylytes have a remanence to saturation strength ratio (Mr/Ms) greater than 0.1, where most host rocks are less than 0.1. Similarly, the Bcr/Bc ratio for most pseudotachylytes is above 3.7, where as it falls below 3.7 for most host rocks. However, the lowest Bcr/Bc ratio measured was pseudotachylyte chip 1740-PST 1, a noteworthy specimen for it's anomalously high values of both Bc (27.2 mT) and Bcr (81.5 mT).

Table 2.2. Compositional measurements for EDS sites reported in Figure 2.4. All reported values are by atom percent. For example, pure magnetite (Fe_3O_4) would be reported Fe = 42.86%, O = 57.14%. Table is organized by pane (A-D) in Figure 2.4. In small, neoformed magnetite grains there is some contamination coming from a measurement volume that extends beyond the grain boundary.

Measurement	Fe %	O %	Si %	Zr %	P%	Interpretation
(A) NE-212						
1	43.19	56.72	-	-	0.09	magnetite
(B) NE-6 15-4 XZ						
1	42.4	57.16	0.45	-	-	magnetite
(C) AZ UW 12 MI-4 YZ						
1	-	67.28	16.48	16.24	-	zircon
2	43.41	56.59	-	-	-	magnetite
(D) NE-6 15-4 XZ						
1	-	67.14	16.81	16.06	-	zircon
2	-	66.61	17.18	16.21	-	zircon
3	42.28	57.72	-	-	-	magnetite
4	42.65	57.35	-	-	-	magnetite

2.4.3 Anisotropy

Anisotropy of Magnetic Susceptibility (AMS)

Bulk susceptibility results show that there are strong magnetic fabrics within our specimens, with consistent orientation between specimens. The direction of maximum susceptibility lies geographically near horizontal (Fig. 2.7). The direction of maximum susceptibility (k1) has low inclination, and declination clusters at 90° increments of declination, suggesting that maximum and intermediate (k2) susceptibility may be similar. Minimum susceptibility (k3) is sub-vertical, and the means for host rock and pseudotachylyte overlap. The average orientation of pseudotachylyte veins reported in Smith (2013) is denoted by the red dashed plane in (Fig. 2.7A). Though the maximum susceptibility directions fall in orientations that may be contained within the plane of pseudotachylyte veins, there is no quantifiable difference between the pseudotachylyte and host rocks, implying that this may be a coincidence. However, the host rock may mylonitized in the same regional stress regime as the pseudotachylytes formed in, so it is plausible that separate AMS fabrics with indiscernible differences were formed by different processes in the host rock and pseudotachylyte veins. If the fabric we observe in magnetic susceptibility is present in the remanence carrying grains as well then our demagnetization data may require a remanence anisotropy correction.

Anisotropy of ARM (AARM)

We quantified remanence anisotropy using the degree (P) and shape (U), defined by the eigenvalues of the anisotropy tensor, k_1, k_2, k_3, where $k_1 \geq k_2 \geq k_3$. P is the ratio of the maximum to the minimum eigenvalue, $\frac{k_1}{k3}$, and $U = \frac{2*k_2-k_1-k_3}{k_1-k_3}$. The shape factors are shown in Figure 2.8. U can vary between -1 and 1, where $U < 1$ indicates a prolate anisotropy ellipsoid and $U > 1$ indicates an oblate anisotropy ellipsoid. The degree of anisotropy must be greater than one; there are fewer outliers in anisotropy degree at higher coercivity windows.

Table 2.3. Table of hysteresis and backfield data for 24 specimens. Specimen NE-1777-5 P X is the same as specimen NE-1777-5 P, oriented with the X-axis parallel to the field instead of the Z axis. Specimen names beginning with 'NE' are oriented cores with demagnetization data, specimen names beginning with a number (eg '1723') and small chips intended to contain entirely either pseudotachylyte or host. Bolded samples have corresponding MPMS data.

specimen	**Ms [Am/kg]**	**Mr [Am/kg]**	**Mr/Ms**	**Bc [mT]**	**Bcr [mT]**	**Bcr/Bc**
1723-Host 1	1.01	0.09	0.08	9.46	32.23	3.40
1723-Host 2	0.84	0.08	0.10	11.74	38.04	3.24
1723-Host 3	0.93	0.10	0.11	12.07	41.10	3.40
1723-host MPMS	**0.88**	**0.06**	**0.07**	**9.25**	**35.11**	**3.80**
1723-PST	**1.46**	**0.16**	**0.11**	**14.53**	**58.84**	**4.05**
1723-PST-2	1.15	0.15	0.13	16.00	59.83	3.74
1723-PST-3	1.10	0.14	0.12	19.06	72.17	3.79
1723-PST-4	1.11	0.16	0.15	16.89	57.16	3.38
1740-Host 1	0.98	0.07	0.07	7.67	26.39	3.44
1740-Host 2	0.83	0.06	0.07	7.85	28.69	3.66
1740-Host 3	0.84	0.06	0.07	7.75	27.75	3.58
1740-host MPMS	**0.80**	**0.06**	**0.07**	**7.43**	**25.92**	**3.49**
1740-PST 1	**0.49**	**0.08**	**0.17**	**27.24**	**81.46**	**2.99**
NE-1723-5 H2	0.86	0.08	0.09	10.96	35.87	3.27
NE-1740-3 H2	0.52	0.05	0.09	10.81	35.59	3.29
NE-1740-3 P	0.78	0.08	0.10	13.84	55.30	3.99
NE-1765-3 P	1.01	0.12	0.12	13.37	52.17	3.90
NE-1765-4 P	0.93	0.10	0.10	11.88	48.54	4.09
NE-1777-1 P	0.96	0.08	0.08	10.02	36.17	3.61
NE-1777-2 H1	0.88	0.05	0.06	6.24	22.61	3.62
NE-1777-2 P	1.01	0.09	0.09	9.32	33.20	3.56
NE-1777-4 H1	0.87	0.06	0.07	7.03	23.84	3.39
NE-1777-5 H1	1.07	0.07	0.07	6.56	22.30	3.40
NE-1777-5 P	0.99	0.10	0.10	12.24	45.28	3.70
NE-1777-5 P X	0.84	0.07	0.08	12.93	53.60	4.15

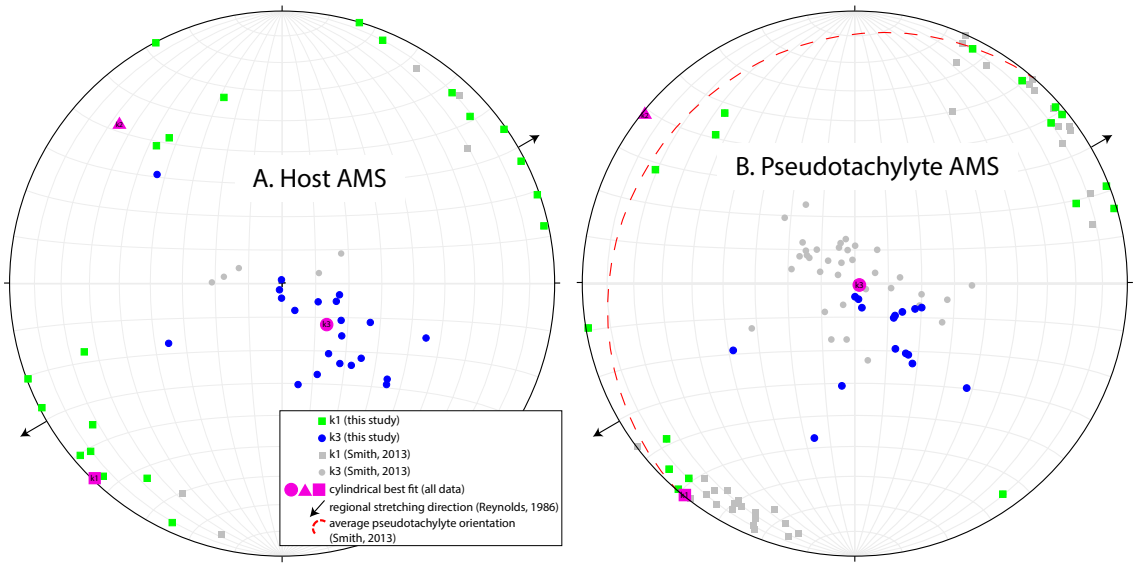

Figure 2.7. AMS maximum (k1) and minimum (k3) directions are consistent between host and pseudotachylyte specimens. Maximum susceptibility axes fall typically within 15° of geographically horizontal, and cluster at 90° declination increments, suggesting an oblate fabric; minimum susceptibility is directed geographically down. Data from pseudotachylytes at the same field location published by Smith (2013) are included in grey, the average pseudotachylyte vein orientation from the same study is the dashed red plane. In magenta are cylindrical best fits for for the combined data from Smith (2013) and this study.

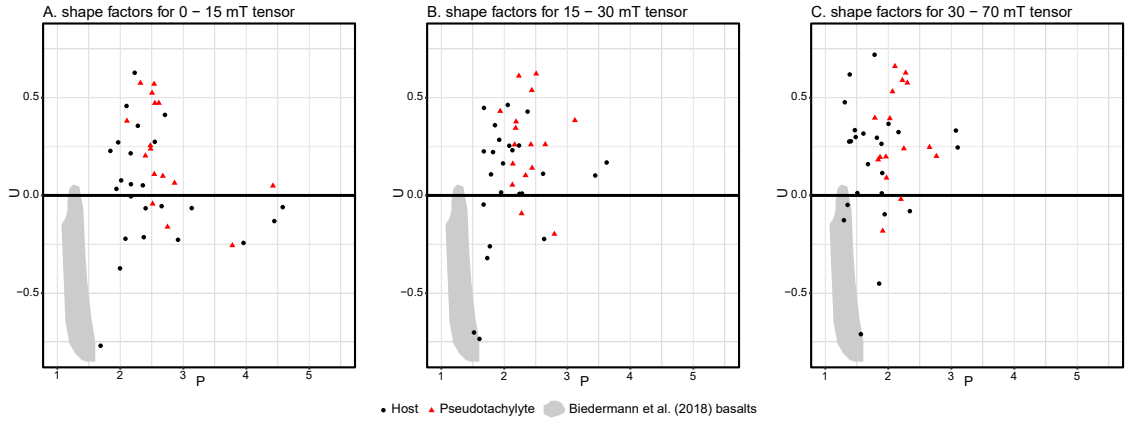

Figure 2.8. AARM shape parameters for each specimen by coercivity window. Shape factor U > 0 indicates an oblate fabric (k1 > k2 >> k3), and U < 0 indicates a prolate fabric (k1 >> k2 > k3).Degree of anisotropy, P, increases to the right. Red triangles represent pseudotachylyte and black squares are host rock. At higher coercivity windows both pseudotachylyte and host rock become more oblate, while the average degree of anisotropy decreases. Grey shaded region is data for context, obtained from Biedermann et al. (2018), from which many of the anisotropy methods used in this study are borrowed. Summary statistics are reported in Table 2.4.

Table 2.4. Summary statistics for anisotropy parameters reported in Figure 2.8.

	0 - 15 mT		15 - 30 mT		30 - 70 mT		AMS	
	P	U	P	U	P	U	P	U
NE-1723								
PST Avg	**2.44**	**0.42**	**2.34**	**0.33**	**2.17**	**0.34**	**1.35**	**0.42**
Host Avg	**2.33**	**0.26**	**2.05**	**0.3**	**1.84**	**0.12**	**1.31**	**0.42**
NE-1723-1 P	2.61	0.47	2.65	0.26	2.30	0.58	1.40	0.41
NE-1723-2 H2	2.16	0.22	1.92	0.28	1.94	-0.10	1.29	0.39
NE-1723-2 P	2.32	0.58	2.19	0.38	2.25	0.24	1.34	0.50
NE-1723-3 H1	2.17	0.06	1.82	0.22	1.68	0.16	1.27	0.35
NE-1723-3 P	2.40	0.20	2.18	0.35	1.96	0.20	1.32	0.35
NE-1723-4 H1	2.71	0.41	2.37	0.43	1.82	0.30	1.39	0.49
NE-1723-5 H2	2.28	0.36	2.08	0.25	1.90	0.11	1.32	0.43
NE-1740								
PST Avg	**2.44**	**0.32**	**2.26**	**0.41**	**1.99**	**0.53**	**1.35**	**0.52**
Host Avg	**2.46**	**0.07**	**2.00**	**0.18**	**1.82**	**0.20**	**1.35**	**0.32**
NE-1740-1 P	2.55	0.47	2.44	0.54	2.11	0.66	1.39	0.6
NE-1740-2 P	2.68	0.10	2.42	0.26	2.07	0.53	1.37	0.46
NE-1740-3 H1	2.66	-0.05	1.98	0.16	1.90	0.01	1.38	0.28
NE-1740-3 H2	2.17	0.00	1.79	0.11	1.41	0.28	1.31	0.02
NE-1740-3 P	2.11	0.38	1.93	0.43	1.79	0.40	1.30	0.50
NE-1740-4 H1	2.55	0.27	2.23	0.26	2.16	0.32	1.36	0.46
NE-1777								
PST Avg	**2.71**	**-0.05**	**2.25**	**0.02**	**1.97**	**0.10**	**1.39**	**0.23**
Host Avg	**2.30**	**-0.11**	**2.02**	**-0.02**	**1.48**	**0.06**	**1.33**	**0.14**
NE-1777-1 H2	2.37	-0.21	2.28	0.01	1.85	-0.45	1.35	0.23
NE-1777-1 P	2.51	-0.04	2.13	0.06	1.91	-0.18	1.36	0.35
NE-1777-2 H1	2.36	0.05	2.13	0.23	1.31	0.48	1.32	0.00
NE-1777-2 P	2.86	0.07	2.34	0.10	2.02	0.40	1.41	0.20
NE-1777-4 H1	2.40	-0.07	1.95	0.02	1.47	0.33	1.36	0.14
NE-1777-5 H1	2.08	-0.22	1.73	-0.32	1.29	-0.13	1.29	0.10
NE-1777-5 P	2.75	-0.16	2.27	-0.09	1.97	0.09	1.39	0.14

AARM angular and intensity deviations

The angular deviation in a sample refers to how far the recorded direction may vary from the applied field direction. This effect is due to remanence anisotropy, and the angular deviation changes based on the orientation of the magnetizing field with respect to the principal axes of the tensor. The anisotropy tensor can be visualized by making a contour map of angular deviation. The deviation is zero by definition along the principal axes, but may be as large as 30° for other orientations. For example, in Figure 2.9 A angular deviation is low ($< 5°$) if the magnetizing field has inclination close to 90°. On the other hand, if declination is 90° and inclination is 50°, the recorded vector may be more than 20° from the true applied field direction. We display angular deviation for NE-1740-3 P, a representative pseudotachylyte specimen with a stable demagnetization path until 70 mT.

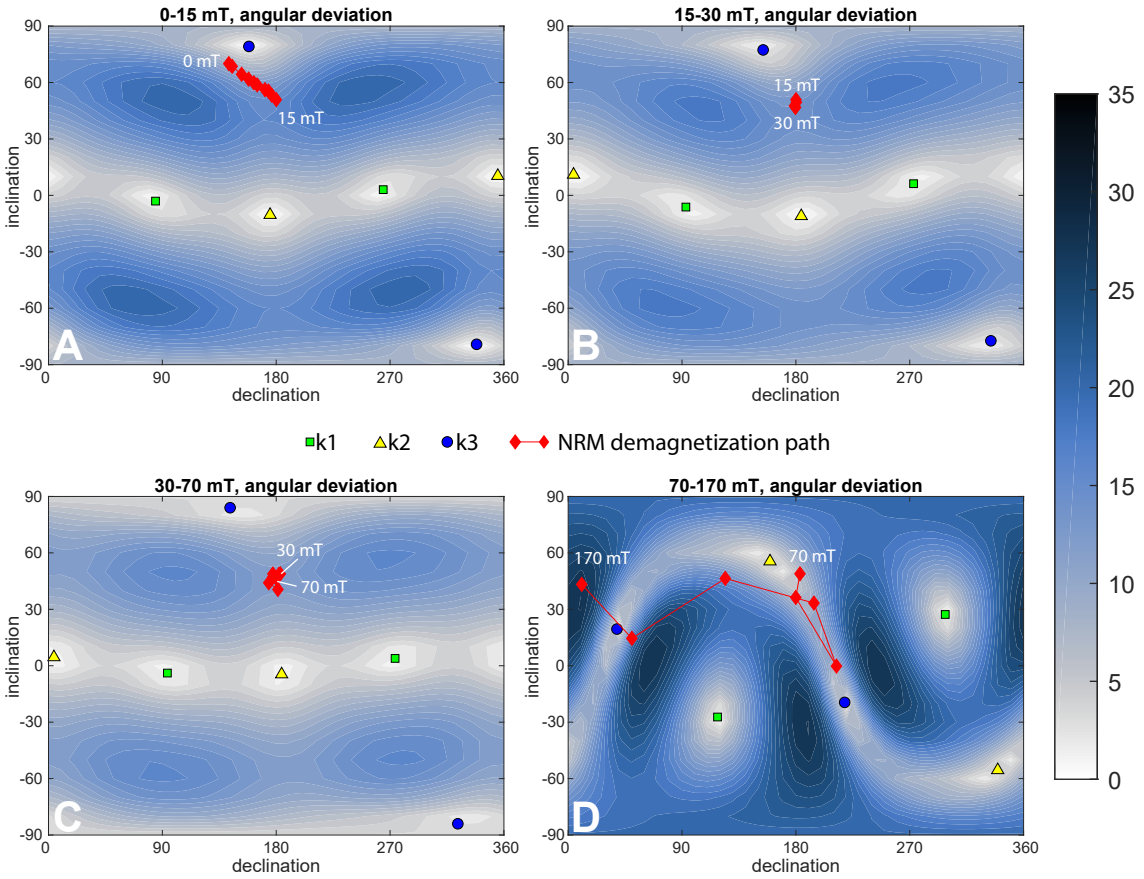

Figure 2.9. Angular deviation by coercivity window for specimen NE-1740-3 P. The broad pattern of high and low deviation is similar in (A), (B), and (C), but looks very different in (D), attributed to the very small fraction of initial remanence remaining by 70 mT. The pattern in the first three panels contains a band of the lowest angular deviation containing k1 and k2 around inclination = 0°, with two other regions of low angular deviation containing k3 perpendicular to them at inclination = 90° and −90°. Demagnetization paths tend to avoid regions of highest angular deviation, but still may be recording 10° to 15° of angular deviation. Recording directions appear to be independent of the principal susceptibility axes.

AARM correction for remanence direction

AARM tensors are used to correct AF demagnetization data for remanence anisotropy. Qualitatively, we determined that demagnetization behavior in our samples changed at 15 mT, 30 mT, and 70 mT; we measured AARM tensors for each specimen corresponding to these coercivities using the protocol described by Biedermann et al. (2019). Each AARM corrected value is calculated using the measured vector and the AARM tensor as described in Chapter 1, linearly interpolating at coercivity values between tensors.

Before applying this method to NRM directions, we tested it with laboratory ARM magnetizations imparted to our specimens directly along the Z axis of the samples in a 50 μT bias field. Initial deflections of up to 30° are an indicator that there is a significant remanence anisotropy (Fig. 2.10).

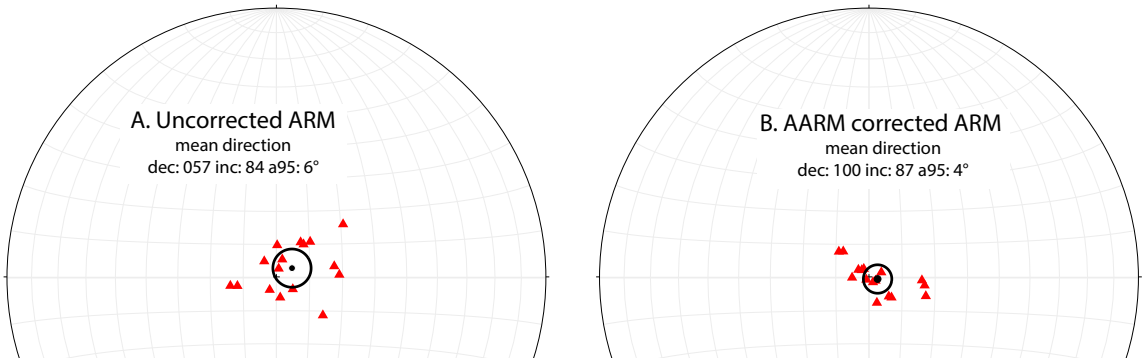

Figure 2.10. ARM initial directions before (A) and after (B) AARM correction. Initial magnetizing field 50μT along z-axis (000, 90). (A) Uncorrected ARM data from pseudotachylyte samples. Deflections as high as 30° from known direction. At a95 confidence, mean of all initial directions barely overlaps with known magnetization direction. (B) AARM corrected data initial directions. Deflections are still evident as high as 20° from known field direction, but the mean of all directions includes the magnetizting direction easily at a95 confidence.

At 95% confidence, the known acquisition direction coincides with the boundary of our confidence window. Upon correction, directions rotated towards the Z axis in a statistically significant way, showing that our corrections were impactful. This rotation can also be observed in an orthogonal vector endpoint diagram for individual samples. We can qualitatively determine the effectiveness of the correction using this orthogonal vector endpoint diagram, where successful AARM corrections will increase alignment with the vertical axis and lengthen the overall vector in this direction near the minumum principal axis (Fig. 2.11).

The results of the coercivity-windowed AARM correction on NRM demagnetizations are shown for various specimens. Figure 2.12C,D shows the correction for a specimen that recorded similar magnetizations at low and high coercivities. The path is generally straightened and the magnetization intensity increased. In Figure 2.14C,D we see that there is no substantial change in the highly curved demagnetization path after AARM correction, though the magnetization intensity is increased. Despite subtle improvements to the demagnetization paths of many samples, the characteristic remanent magnetization (ChRM) directions do not substantially change as a result of our anisotropy corrections. Thus, we see little difference in the sample mean directions we are comparing to the reference direction.

2.4.4 Natural remanent magnetizations

AF demagnetization

Most specimens in this study lost remanence early in AF demagnetization experiments. The majority of remanence was held at less than 10 mT even in pseudotachylyte veins. However, we determined experimentally that the magnetization held at low coercivities may be less reliable than that held at higher coercivities. Where possible, our analysis of remanence directions therefore uses only the high-coercivity component of magnetization. However, in some specimens the two

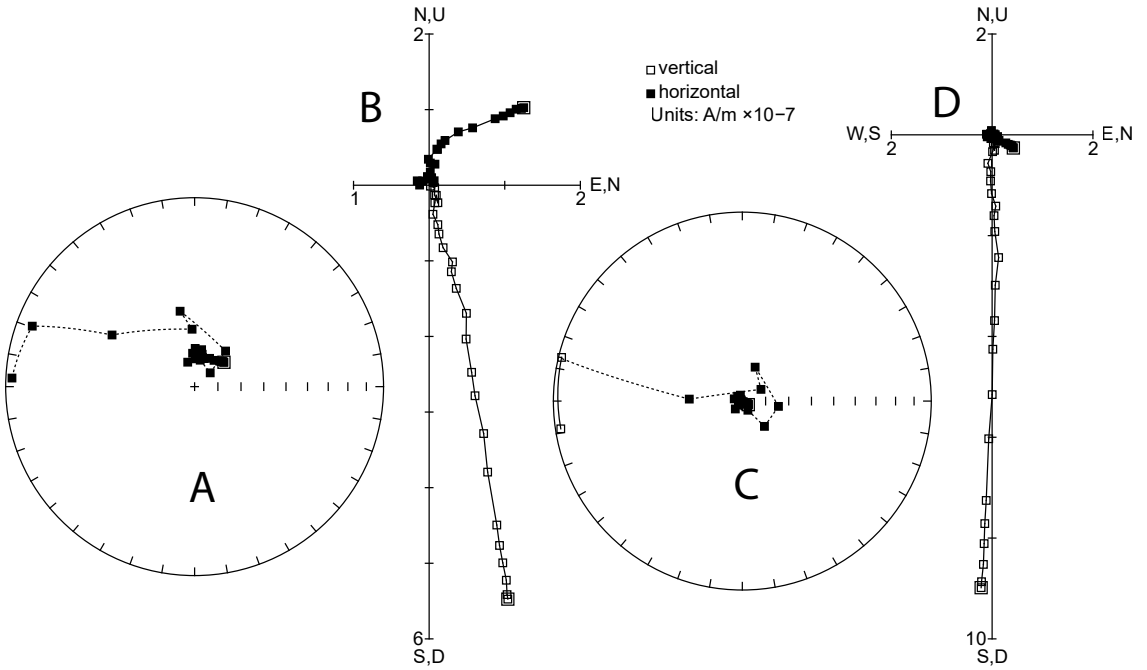

Figure 2.11. AARM correction of ARM magnetization on specimen NE-1777-2 P. (A) and (B) are pre-correction and (C), (D) are post-correction. The magnetization was imparted along the vertical axis, the middle of the stereonet in (A), (C) and along the vertical axis in (B), (D). The dramatically improved fit with the expected direction after correction is evidence that our AARM correction is effective.

components are not discernible so all data are used.

Specimen NE-1740-1 P (Fig. 2.12) is an example of low coercivity and high coercivity components holding roughly the same remanence direction. The ChRM direction using the points from 30 mT to 60 mT is 315/66, while the ChRM direction obtained from the 1 - 30 mT data is 312/70. Regardless, for consistency we have used only the high coercivity points to determine a direction for specimens of this sort. The median destructive field of this specimen is 13 mT, which is slightly above average.

In contrast, remanence directions in specimen NE-1723-2 P (Fig. 2.13) are vastly different at low and high coercivities. The low coercivity component ($<$ 15 mT) records 066/-20, while the high coercivity component (25 mT to 60 mT) records 161/-62. The high coercivity component is a close match to the reference direction, while the low coercivity component is not. The median destructive field is 20 mT.

For some specimens, remanence is lost so quickly that there is no high coercivity component at all. NE-1777-2 P (Fig. 2.14), representative of all NE-1777 specimens, has a median destructive field of just 4 mT and lost essentially all magnetization by 20 mT. While there appears to be multiple components of magnetization, shown by the curved demagnetization path, there is no stable component at high coercivity. For this and similar specimens, we fit great circles to the data at all coercivities up to the point where the contribution of noise is similar to that of signal. The ChRM direction lies somewhere along the great circle.

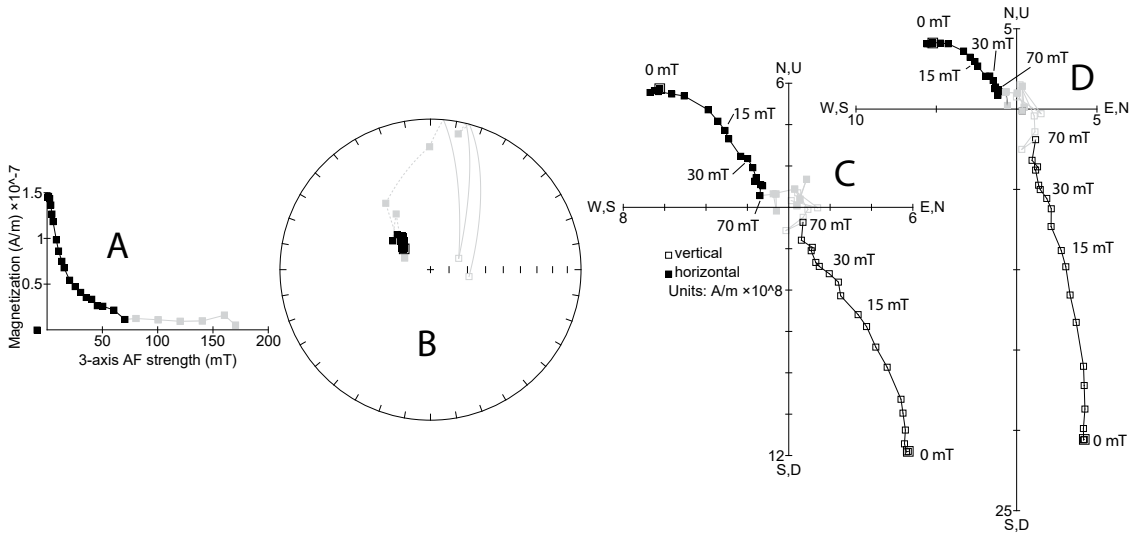

Figure 2.12. AF demagnetization of NRM in NE-1740-1 P, shown in geographic coordinates. Low and high coercivity grains record similar remanence directions. (A) magnetization intensity at each AF demagnetization step; (B) equal area net showing AARM corrected demagnetization data; (C) orthogonal vector endpoint diagram (OVED) of NRM demagnetization; (D) AARM corrected OVED of NRM. Hollow squares on the stereonet are upper hemisphere, solid squares are lower hemishpere. Grey data points are demagnetization steps in a field greater than 70 mT. At these high coercivities, we consistently see more noise than signal in our specimens.

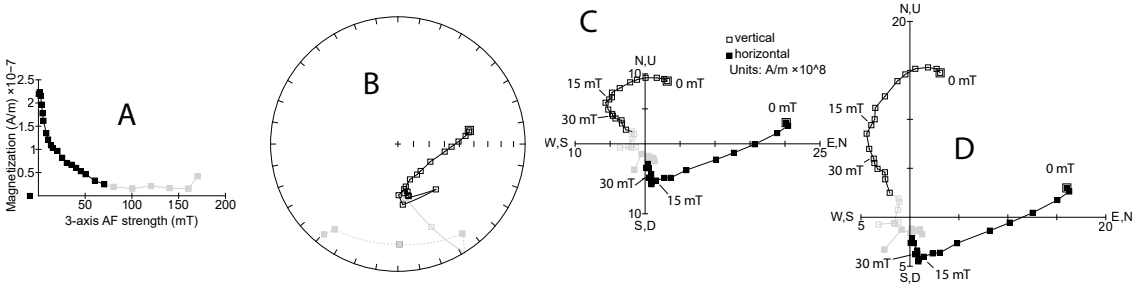

Figure 2.13. AF demagnetization of NRM in NE-1723-2 P with distinct low-coercivity and high coercivity components that record different magnetization directions. Symbols and lettering the same as Figure 2.12

Thermal

Demagnetization paths from thermal demagnetization experiments are of varying quality. In general, pseudotachylyte specimens produce more linear trends than their associated hosts, as in sample NE-1740 (Fig. 2.15). Sample NE-1777 produced generally linear (and highly similar) demagnetization paths in both host and pseudotachylyte (Fig. 2.16), and specimen NE-1723 had two of three pseudotachylyte specimens yield fairly linear paths, while the third and both host specimens were of lower quality (Fig. 2.17).

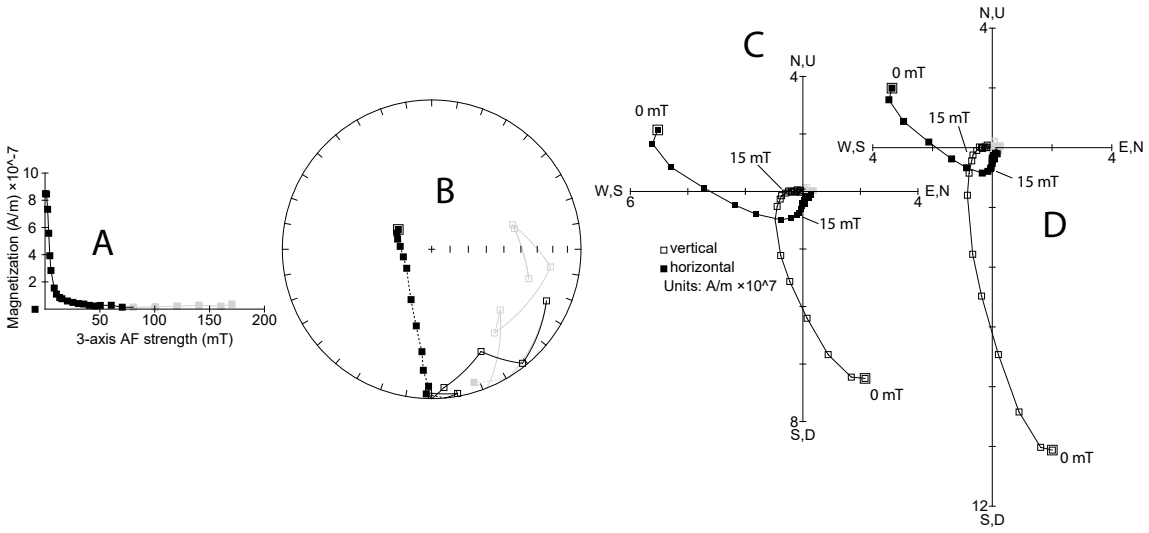

Figure 2.14. AF demagnetization of NRM in NE-1777-2 P, which loses most of its remanence at very low fields. Symbols and lettering are the same as in Figure 2.12.

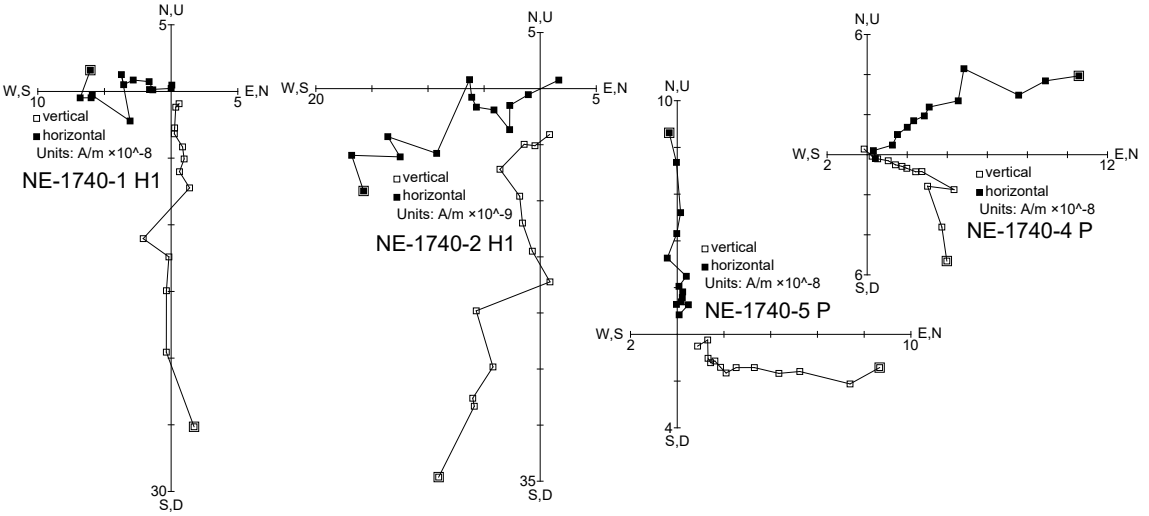

Figure 2.15. Orthogonal vector endpoint diagrams showing thermal demagnetization of two host and two pseudotachylyte specimens from sample NE-1740. The host specimens have a weak linear fit, while the pseudotachylyte specimens are more linear. There is one outlier point at 200°C in NE-1740-4 P. The initial data point was measured at room temperature, then data were collected every 50°C from 100°C to 650°C.

Remanence directions

Several specimens were taken from the pseudotachylyte vein in each hand sample. The mean direction of several specimens from each vein was used when evaluating agreement with the expected reference direction. Of the six samples for which we obtained demagnetization data from pseudotachlylyte veins, only three had enough coherent data to produce sample means for both

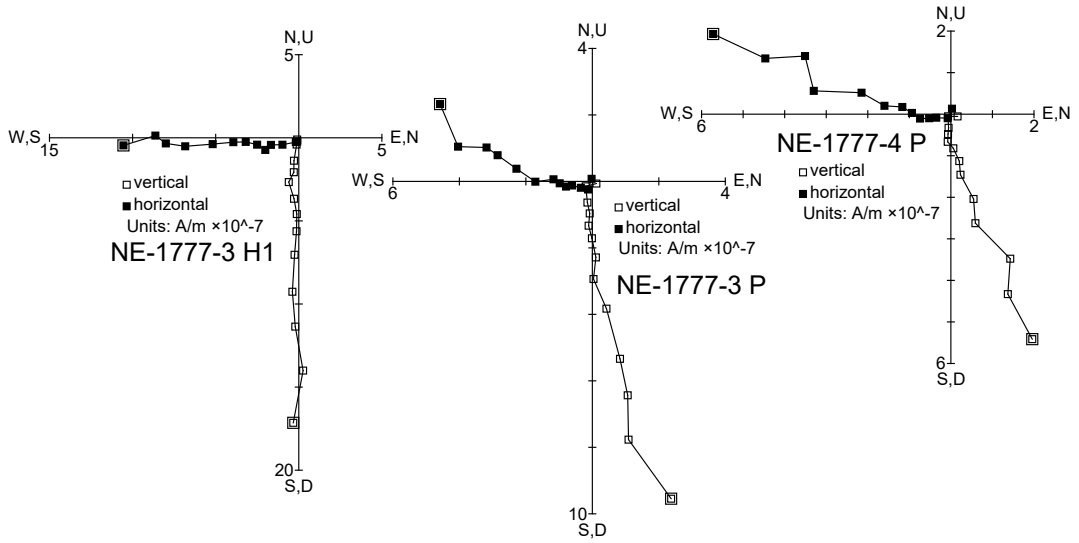

Figure 2.16. Orthogonal vector endpoint diagrams showing thermal demagnetization of one host and two pseudotachylyte specimens from sample NE-1777. All specimens have a fairly linear demagnetization path. The initial data point is measured at room temperature, then data is collected every 50°C from 100°C to 650°C.

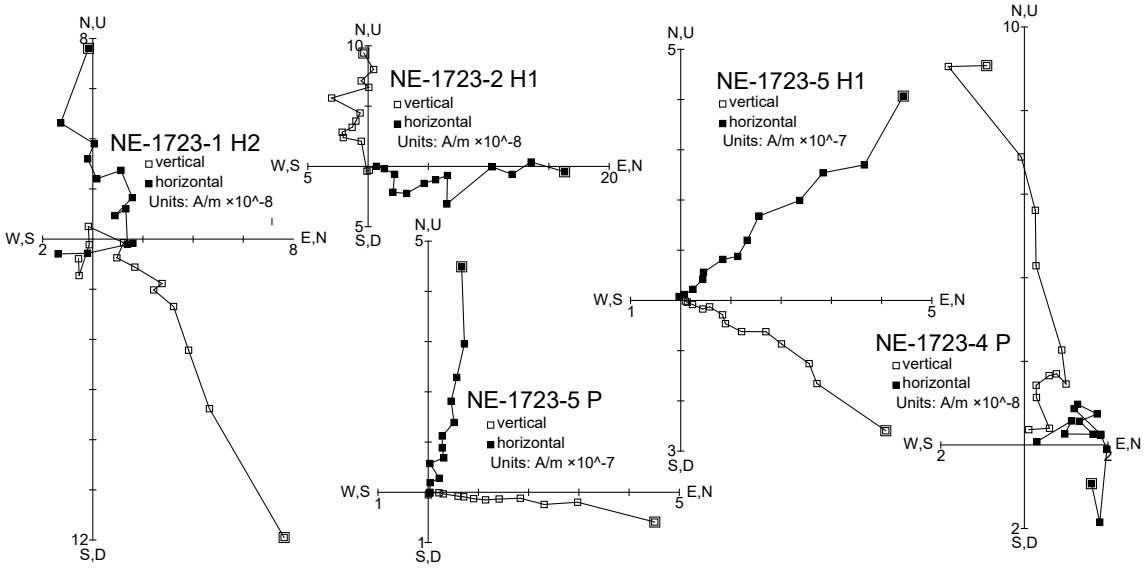

Figure 2.17. Orthogonal vector endpoint diagrams showing thermal demagnetization of three host and two pseudotachylyte specimens from sample NE-1723. The host data are largely non-linear, while two of the three pseudotachylyte specimens exhibit linear behavior. The initial data point is measured at room temperature, then data is collected every 50°C from 100°C to 650°C.

pseudotachylyte and host rock: NE-1723, NE-1740, and NE-1777. All three resulted in vein-average directions that coincided at least approximately with a reference direction (Fig. 2.18).

Notably, though sample sizes were small, we did not see overwhelming agreement between our

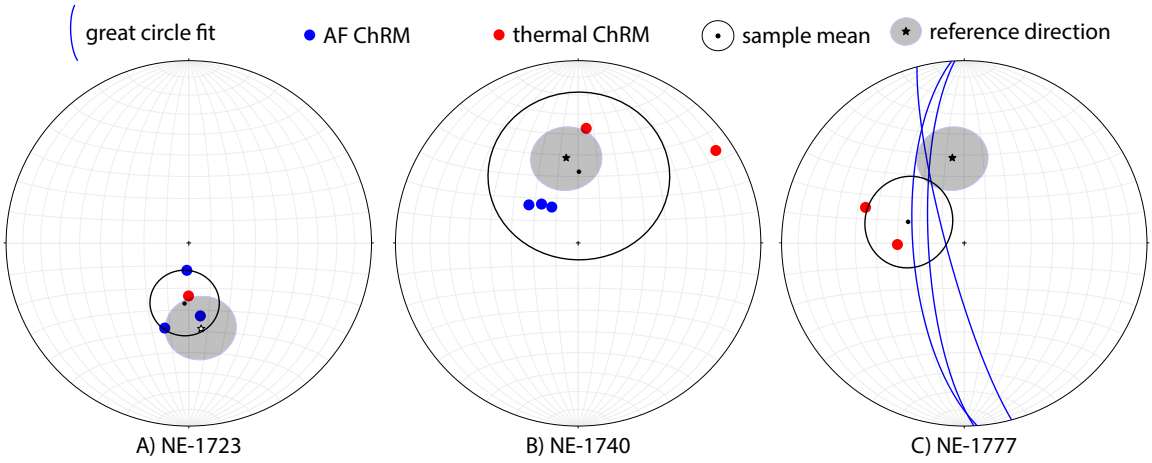

Figure 2.18. Specimen ChRM and sample means for pseudotachylyte veins (A) NE-1723, (B) NE-1740, and (C) NE-1777. Reference directions are included, blue indicates a ChRM direction obtained from AF demagnetization, red from thermal demagnetization.

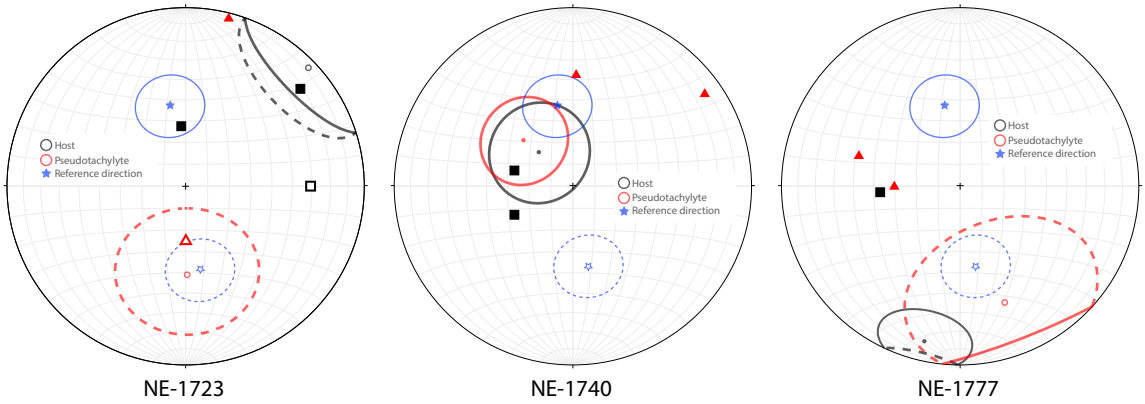

Figure 2.19. ChRM directions from thermal demagnetizations overlain onto the sample means from AF-demagnetization. Pseudotachylytes specimens red triangles, host rocks are black, and the reference direction is shown in blue for both normal and reverse polarity with a 15° error ellipse. While some specimens fall near or within the AF sample means, many are well outside.

AF and thermal demagnetization data. Comparing mean directions of AF data to ChRM directions from thermal demagnetizations shows that rarely do the ChRM directions overlap with our 95% confidence windows (Fig. 2.19). Despite this, the overall mean directions reported in (Fig. 2.18) all show rough agreement with the reference direction.

IRM

We imparted 60 mT isothermal remanent magnetizations (IRMs) to our samples to mimic the magnetizations that rocks may acquire when they are struck by lightning. The results of IRMs imparted to our samples are presented below, and their implications for lightning-induced secondary magnetizations will be discussed later. IRM magnetization intensities are two to three orders of

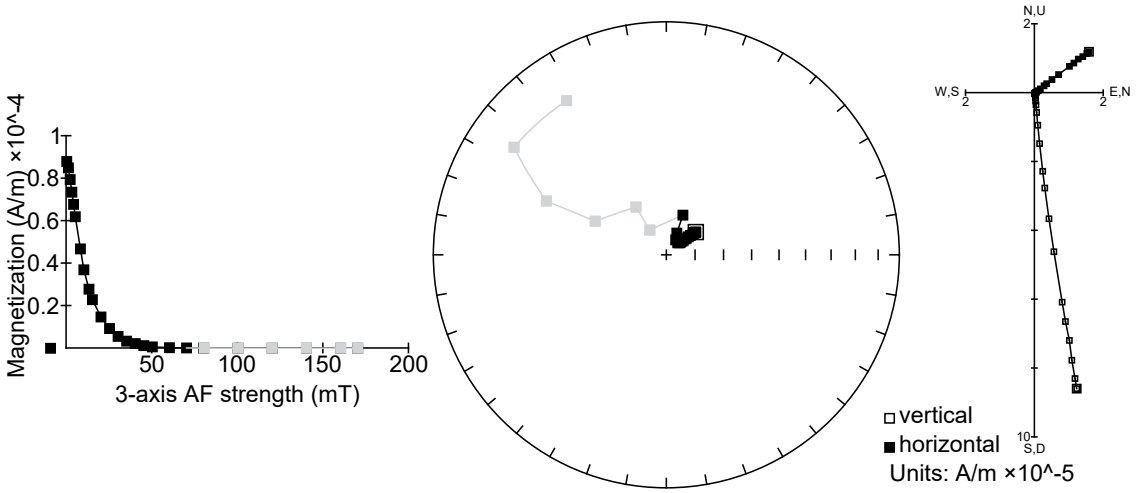

Figure 2.20. Demagnetization of IRM in specimen NE-1777-2 P acquired parallel to z-axis (000, 90). There is a minor deflection of about 10° between the recording direction and the acquisition direction, and IRM intensity is 100 times stronger than NRM intensity. This specimen exhibited multi-component behavior during NRM demagnetization (Fig. 2.14). Symbols the same as Figure 2.12.

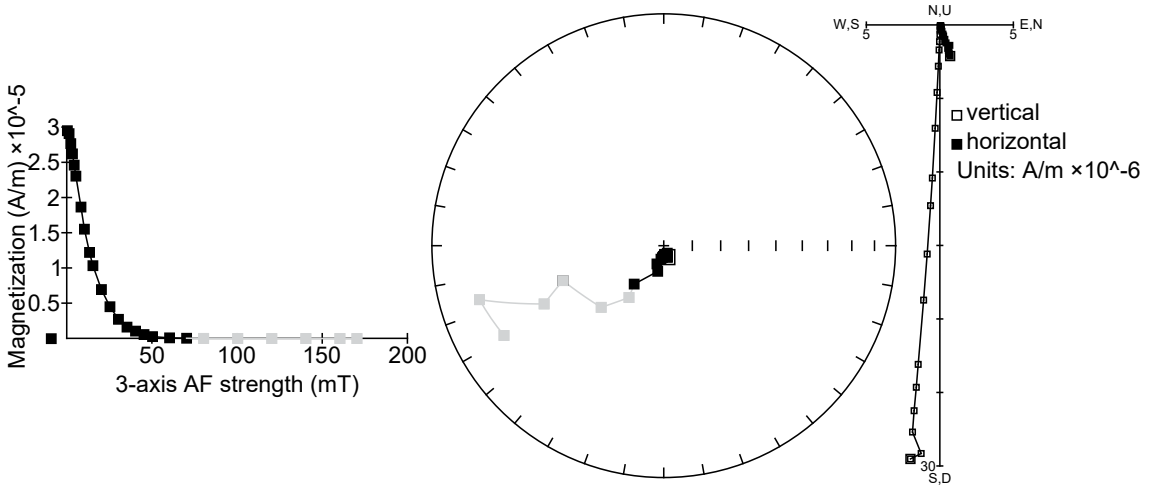

Figure 2.21. Demagnetization of IRM in specimen NE-1740-1 P acquired parallel to z-axis (000, 90); the recording direction is deflected less than 5° from the acquisition direction. The magnetization intensity is 200 times stronger than the NRM intensity. The NRM for this specimen is single component (Fig. 2.12). Symbols the same as (Fig. 2.12).

magnitude greater than both ARM and NRM intensities, and the mean deflection is smaller. At the specimen level, there are still some samples with quite large deflections (Fig. 2.20), but overall many have smaller deflections $\leq 10°$ (Fig. 2.21). The strong magnetizing field used to impart these IRMs universally produced the same recording direction in both low coercivity and high coercivity grains.

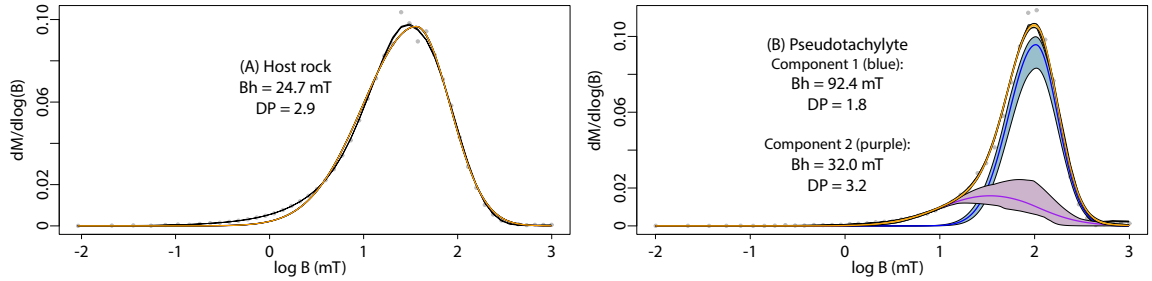

Figure 2.22. Coercivity unmixing for NE-1740, using specimens 1740-host MPMS and 1740PST-1. Components are compared to a smoothed, least-squares fit of backfield data. (A) Host rock unmixing gives a single, slightly skewed component with medium dispersion, attributed to the large, MD magnetite grains in the host rock. (B) Pseudotachylyte unmixing gives two components, consistent with the bimodal distribution of magnetic grain sizes. A single, compact, and symetric component with high coercivity is the result of the small, neo-formed magnetite grains. A low coercivity, symmetric but highly dispersed component is the result of the surviving host magnetite grains within the pseudotachylyte.

2.5 Discussion

2.5.1 Coercivity unmixing

Using the MaxUnmix program by Maxbauer et al. (2016), we unmixed the remanence coercivity spectra for our samples. Host rocks were able to be adequately described using only one component, while two components better described pseudotachylyte specimens; one with a coercivity similar to the single component used for host specimens, and one with a significantly higher coercivity (Fig. 2.22). The single, soft component used for host specimens reflects the large, multi-domain magnetite grains present in the host material. The similar component observed in pseudotachylyte specimens can be attributed to relict host magnetite grains that remain within the pseduotachylyte zone, whereas the hard component seen only in the pseudotachylyte specimens is from the small, neoformed magnetite grains that crystallized during rapid melt quenching. The rapid cooling conditions that formed these grains explains why they are only seen in the pseudotachylyte specimens, while the lower-coercivity component from grains that originated in the host rock is seen in both host and pseudotachylyte specimens because of the prevalence of original host inclusions within pseudotachylyte melts. Figure 2.23 shows how the coercivities and dispersion vary between the different components. The component attributed to neo-formed magnetite within the pseudotachylyte has a much higher coercivity and a narrow distribution. On the other hand, the host magnetite grains, both original and relict, have a much lower coercivity and a high degree of dispersion.

2.5.2 Low temperature remanence data

Low temperature data support our conclusion that there is a single population of magnetite grains in host samples, but two populations of magnetite grains within pseudotachylyte veins where one of the groups originated in the host rock and one nucleated within the pseudotachylyte melt. Figure 2.24A,C demonstrates the dominant Verwey transition in host specimens around 128 K, where

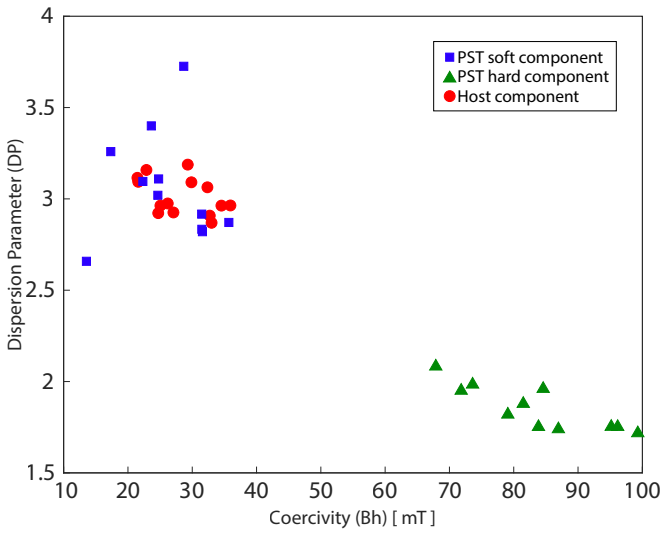

Figure 2.23. Comparison of coercivity (Bh) to dispersion parameter (DP) of remanence components in backfield curves for 25 specimens. Host rocks were described by only one component (red circles), while pseudotachylyte was described by two components: (1) a soft component attributed to relict magnetite grains from the host rock, and (2) a hard component corresponding to the neo-formed magnetite grains in the pseudotachylyte veins. There is an obvious difference in both Bh and DP between the newly-formed grains and the host grains, and in both populations, DP tends to decrease with increasing Bh.

as in pseudotachylyte specimens (Fig. 2.24B,D) there are two Verwey transitions, one at 128 K and one at 108 K. There is some evidence for a lower temperature Verwey transition in the NE-1723 host specimen (Fig. 2.24A), but that be explained by the extreme difficulty separating host rock from pseudotachylyte in our samples. The small magnitude of lower temperature anomaly is likely indicative of a tiny fragment of pseudotachylyte present in our host specimen.

2.5.3 Remanence anisotropy and correction

There is a dichotomy between the apparent effectiveness of our anisotropy of remanence (AARM) correction methods when correcting laboratory ARM magnetizations and NRMs. AARM corrections made statistical improvements to ChRM directions of laboratory ARMs, acquired in a known field (Fig. 2.10), but despite this demonstrated effectiveness we had little success resolving complicated NRM demagnetizations into single recognizable ChRM directions (Fig. 2.14). From coercivity unmixing, we learned that neo-formed magnetite grains within pseudotachylyte veins only hold remanence from the time of crystallization following rupture, whereas larger grains may hold remanence from the time of rupture but also may carry a second component of remanence. For specimens in which anisotropy correction does not resolve the NRM into a single component, it is reasonable to conclude that there are multiple components of magnetization being held within the different grain size populations, and thus the anisotropy correction is effective, though no single component of magnetization is obtained. It is also noteworthy that there are significantly lower degrees of anisotropy

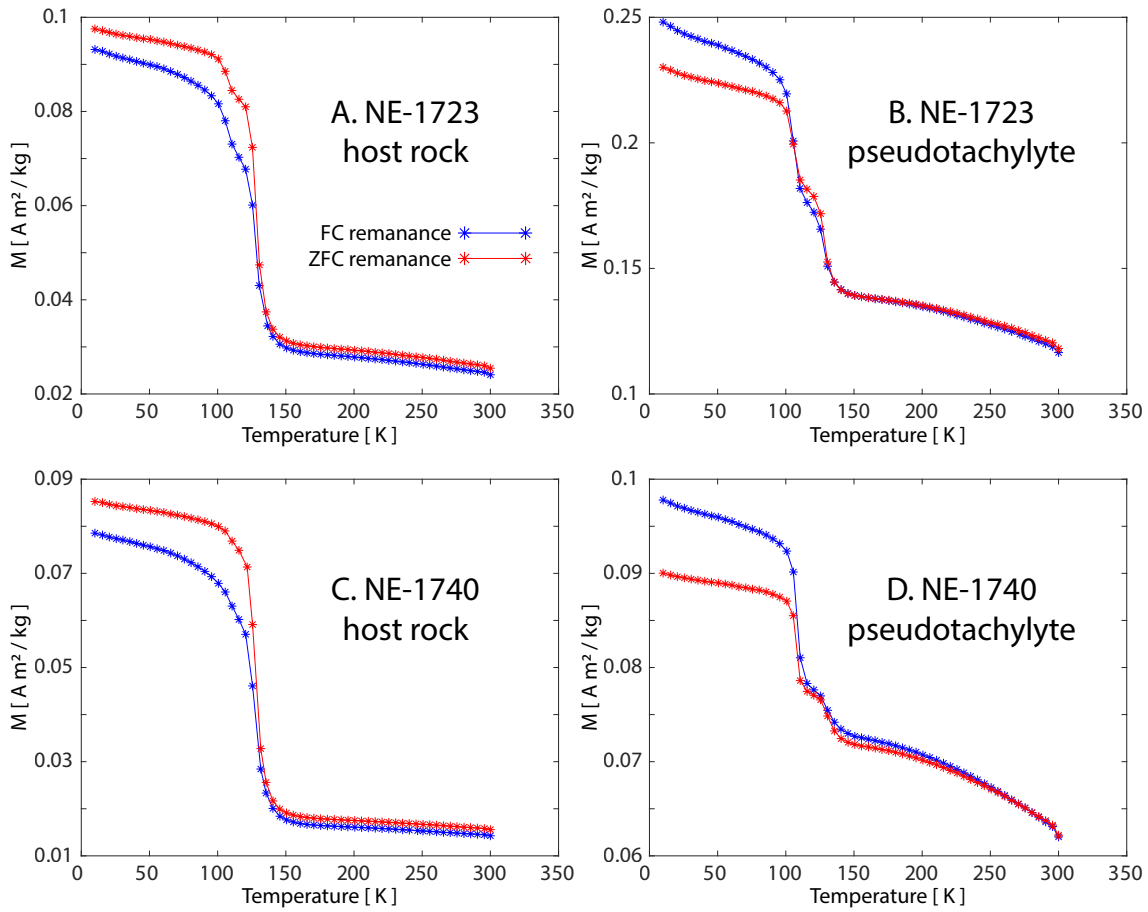

Figure 2.24. Low temperature data from host and pseudotachylyte specimens, contributing to the body of evidence that suggests a population of magnetite grains unique to pseudotachylyte veins, in addition to a shared population of grains present in both host and pseudotachylyte specimens.

at higher coercivities where pseudotachylyte remanence is held (Fig. 2.8).

2.5.4 Possible role of lightning

We demagnetized 57 specimens (40 AF, 17 thermal) from eight hand samples of pseudotachylyte veins, but were only able to obtain sample mean directions for three of the hand samples using just 29 (51%) of the specimens. We rejected three specimens from the three samples for which we were able to calculate mean directions. With the remaining 23 specimens from 5 samples we were unable to obtain mean directions within reasonable error constraints. For some samples, this may be due in part to a small sample size, but the data also suggest that there may be localized factors influencing recording in the hand samples. Lightning strikes are known to remagnetize small volumes of rock, producing anomolously high magnetization intensities and random recording directions. In the analysis below, we conclude that it is highly unlikely that our samples have been affected by lightning of any variety, and that other factors are needed to explain the dispersion we see in our directional data.

Based on location alone, we find the incidence of regular, surface to ground, lightning to be unlikely within the vicinity of our samples, which were collected from a low-lying, recent and man-made exposure. However, our investigation of possible lightning influence also covers a lesser-known type of "earthquake lightning," reported to affect pseudotachylyte veins by Ferré et al. (2005). We expect earthquake lightning to have the same effect on magnetization as conventional lightning, and thus we would not be able to distinguish between the two on the basis of solely magnetic data. However, due to the location of the samples, support for lightning induced magnetizations would more likely be interpreted as support for the earthquake lightning hypothesis.

To explore the potential influence of lightning, we gave each sample an anhysteretic remnant magnetization (ARM) and an isothermal remnant magnetization (IRM). We expect ARM magnetizations to behave similarly to a thermal remnant magnetization (TRM), that would have been acquired by pseudotachylyte and host rocks as they cooled from their melt phase. In contrast, laboratory induced IRMs behave similarly to lightning induced magnetizations from the field. We make comparisons between the magnetic qualities of the NRM and both ARM and IRM to determine which the NRM more resembles.

The initial magnetization intensities of IRMs are orders of magnitude greater than the NRM we measured, which compare favorably to the ARMs (Fig. 2.25). Abnormally high magnetization intensity is a signature of lightning affliction, so these low-intensity results demonstrate that our samples are more consistent with what we would expect for a TRM than an IRM. Additionally, the IRM measured in our samples, though two orders of magnitude greater than the NRM, are still four orders of magnitude less than 200 Am^2/kg reported by Ferré et al. (2005). However, it should be noted that this reported value is suspect because it is twice the saturation magnetization of pure magnetite.

Figure 2.25 displays the initial magnetization intensity by type of magnetization for both pseudotachylyte and host rock. The initial intensity of IRMs is orders of magnitude higher than ARMs or NRMs, the distribution of which roughly overlap. This data refutes the idea that the samples were affected by lightning because we would expect drastically greater magnetization intensities. There is no apparent difference in intensity between pseudotachylyte and the host rock as has been reported by researchers in other areas (Ferré et al., 2005).

2.5.5 Interpretation of remanence

The complete magnetic characterization of our samples informed our ChRM analysis by explaining the changes in demagnetization behavior with coercivity. We recognized a population of low-coercivity magnetite grains within the pseudotachylyte that originated in the host rock, as well as a population of high-coercivity magnetite grains that formed contemporaneously with pseudotachylyte. Where possible in our analysis, we used exclusively the high coercivity magnetite grain population to calculate ChRM directions because of the superior recording properties of smaller, pseudo-single domain grains.

Previous paleomagnetic data were collected from our field site by Smith (2013), but her work lacked the thorough magnetic characterization we have put forth. Thus, part of our work has been re-interpreting the raw data from that study with our improved understanding of the magnetic

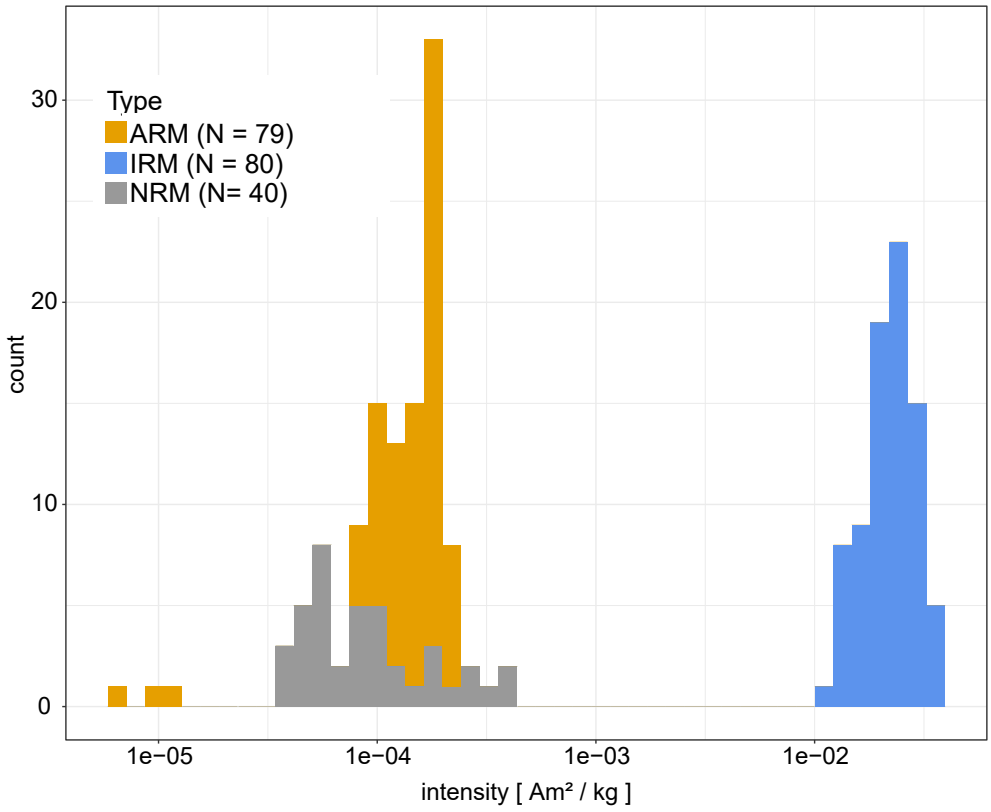

Figure 2.25. Histogram of initial magnetization intensities for samples by type: NRM, ARM, or IRM. Magnetization intensities are displayed on a log-scale along the horizontal axis. The IRM magnetization intensities are orders of magnitude greater than the NRM or ARM intensities, implying that our samples are not affected by lightning.

characteristics of these materials. Figure 2.26 shows the pseudotachylyte means for our three, well characterized pseudotachylyte veins and an additional 10 veins originally measured by Smith (2013), re-interpretted with the same methods as we used for our veins. The means average data from three to six specimens per sample, using both thermal and AF demagnetization techniques. Table 2.5 summarizes our re-interpretation.

The synthesis of data from our study and Smith (2013) gives clear evidence of low-angle activity for nine pseudotachylyte veins; NE-103, NE-104, NE-204, NE-209, NE-212, NE-217, NE-1723, NE-1740, and NE-1777 all coincide with either the normal or reverse polarity reference direction. Three more samples, NE-218, NE-225, and NE-231 are rotated 180° from the reference direction; we find it likely that these samples were misoriented. If north was mislabeled as south on these samples in the field, then these samples would fit into the greater pattern we see at the site and provide support for pseudotachylyte generation at low angles. Of the 13 samples for which we were able to calculate a mean direction only one, NE-206, does not have evidence to support low-angle formation. One sample from Smith (2013) and two from this study had too much variation within each vein to determine a sample mean.

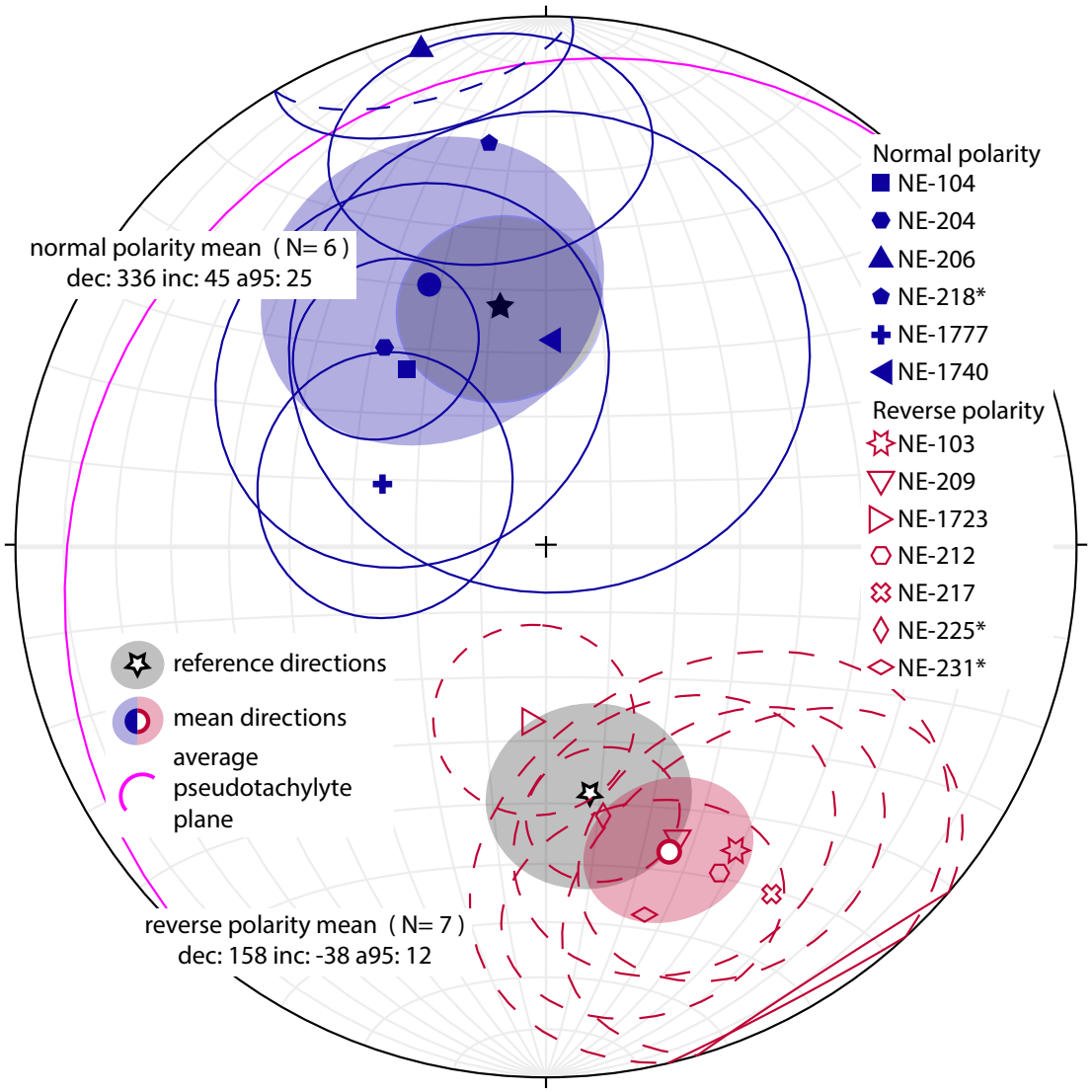

Figure 2.26. Directional means from thermal and AF demagnetization of South Mountains Pseudotachyltes from Smith (2013).

Reversal tests

We performed reversal tests on the combined data set of this paper and Smith (2013), considering three possible scenarios: (1) using all of the sample means as they were calculated, assuming that they are all correctly oriented; (2) the same data as (1), but discarding sample means that may be misoriented; and (3) a best-case scenario where sample means discarded in (2) are rotated 180° so that reverse polarity means are near the reverse polarity reference direction and normal polarity means are all near the normal polarity reference direction. Scenarios (2) and (3) pass the reversal test, while scenario (1) fails. Therefore, it is likely that these two modes of data represent the same

Table 2.5. Summary table of original and reinterpreted data from Smith (2013). Columns 'N AF', 'N T' denote the number of AF or thermal demagnetizations used in (or rejected from) in the mean calculations. * denotes sample that were likely misoriented by 180 degrees in the field.

Sample	dec	inc	a95	N AF	N T	N AF rejected	N T rejected
NE-103	148	-33	22	3	0	0	0
NE-104	322	55	30	0	5	0	0
NE-204	320	50	14	3	1	0	0
NE-206	338	-2	13	4	1	0	1
NE-209	155	-39	23	3	0	0	0
NE-212	152	-34	30	4	0	0	1
NE-217	147	-23	28	4	2	2	2
NE-218*	172	24	21	3	1	0	0
NE-225*	348	-51	20	4	0	1	0
NE-231*	345	-29	19	5	1	2	1
NE-1723	184	-63	15	3	1	0	1
NE-1740	001	58	40	3	2	0	0
NE-1777	291	63	20	3	2	0	0

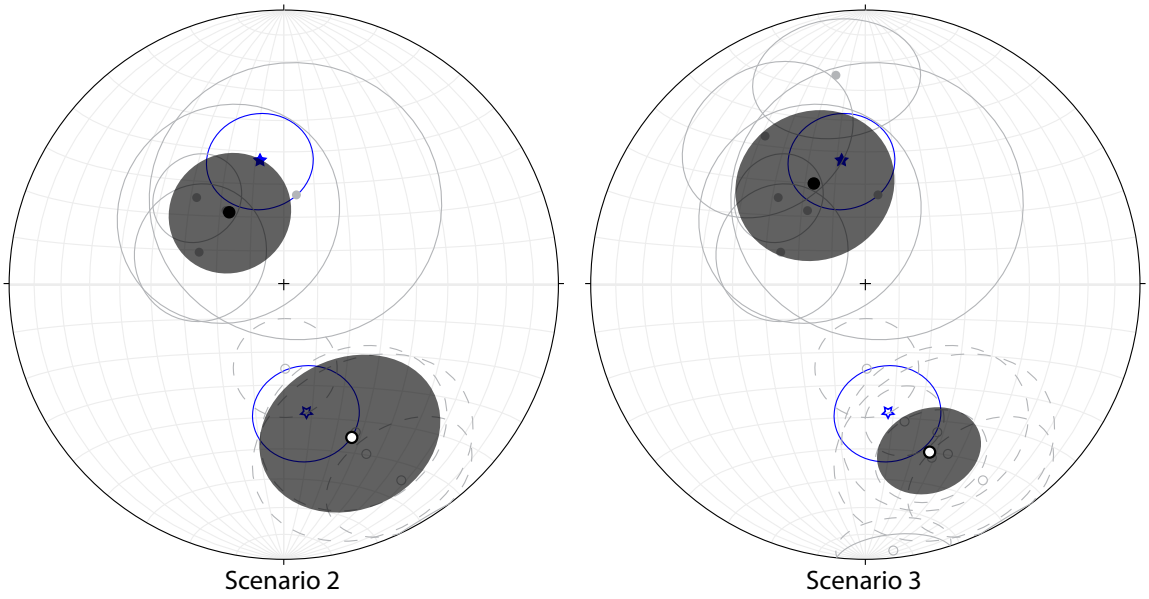

Figure 2.27. Mean of mean directions representing scenarios (2) and (3), discussed in text. Scenario (1) is not shown because mean direction carries too much error. Overall mean of sample means is shown by translucent black circle, sample means are shown by grey outlines. Blue circles and stars show reverse (open star) and normal (filled star) reference directions.

field direction. We still cannot rule out that some of the data reported in Smith (2013) was rotated 180°.

2.6 Conclusions

This study provides strong support for earthquakes along low-angle normal faults, commonly believed to be either seismically inactive or to produce only microseismicity. Eleven of 13 sample means coincide with either the normal or reverse polarity reference direction, as does the mean of all normal polarity means, and the mean of all reverse polarity means. The presence of both normal and reverse polarity events corroborates the evidence, obtained from Argon dating techniques, that suggests this low-angle normal fault system was seismically active over a long period of time.

Bibliography

E. Anderson. The dyamics of faulting and dyke formation with applications to Britain. *Hafner Pub. Co.*, 1951.

J. Besse and V. Courtillot. Apparent and true polar wander and the geometry of the geomagnetic field over the last 200 Myr. *Journal of Geophysical Research: Solid Earth (1978–2012)*, 107(B11): EPM 6–1, 2002. ISSN 2156-2202. doi: 10.1029/2000JB000050.

A. R. Biedermann, D. Bilardello, M. Jackson, L. Tauxe, and J. M. Feinberg. Grain-size-dependent remanence anisotropy and its implications for paleodirections and paleointensities – Proposing a new approach to anisotropy corrections. *Earth and Planetary Science Letters*, 512:111–123, apr 2019. ISSN 0012-821X. doi: 10.1016/J.EPSL.2019.01.051.

W. R. Buck. FLEXURAL ROTATION OF NORMAL FAULTS. *Tectonics*, 7(5):959–973, 1988.

C. Collettini and R. H. Sibson. Normal faults, normal friction? *Geology*, 29(10):927, oct 2001. ISSN 0091-7613. doi: 10.1130/0091-7613(2001)029¡0927:NFNF¿2.0.CO;2.

C. Collettini, A. Niemeijer, C. Viti, and C. Marone. Fault zone fabric and fault weakness. *Nature*, 462(7275):907–910, dec 2009. ISSN 0028-0836. doi: 10.1038/nature08585.

G. A. Davis and G. S. Lister. Detachment faulting in continental extension; Perspectives from the Southwestern U.S. Cordillera. *Geological Society of America Special Papers*, 218:133–160, jan 1988. ISSN 0072-1077. doi: 10.1130/SPE218-p133.

E. C. Ferré, M. S. Zechmeister, J. W. Geissman, N. Mathanasekaran, and K. Kocak. The origin of high magnetic remanence in fault pseudotachylites: Theoretical considerations and implication for coseismic electrical currents. *Tectonophysics*, 402:125–139, 2005. doi: 10.1016/j.tecto.2005.01.008.

E. C. Ferre, J. W. Geissman, and M. S. Zechmeister. Magnetic properties of fault pseudotachylytes in granites. *Journal of Geophysical Research: Solid Earth*, 117, 2012. doi: 10.1029/2011JB008762.

P. G. Fitzgerald, ˜. S. J. Reynolds, E. Stump, D. A. Foster˜, A. J. W. Gleadow' ˜, and . Victorian. THERMOCHRONOLOGIC EVIDENCE FOR TIMING OF DENUDATION AND RATE OF CRUSTAL EXTENSION OF THE SOUTH MOUNTAINS METAMORPHIC CORE COMPLEX AND SIERRA ESTRELLA, ARIZONA. *Nucl. Tracks Radiat. Meas*, 21(4):555–563, 1993.

L. B. Goodwin. Controls on pseudotachylyte formation during tectonic exhumation in the South Mountains metamorphic core complex, Arizona. *Geological Society, London, Special Publications*, 154(1):325–342, 1999. ISSN 0305-8719. doi: 10.1144/GSL.SP.1999.154.01.15.

S. Haines, C. Marone, and D. Saffer. Frictional properties of low-angle normal fault gouges and implications for low-angle normal fault slip. *Earth and Planetary Science Letters*, 408:57–65, 2014. doi: 10.1016/j.epsl.2014.09.034.

J. Hoehn, L. Goodwin, M. Longchamp, J. Feinberg, B. Jicha, B. Singer, D. Smith, and M. Heizler. Pseudotachylyte records earthquakes >M6.0 on low-angle normal faults. In *AGU 2018*, Washintgon, DC, 2018.

J. A. Jackson. Active normal faulting and crustal extension. *Geological Society of London Special Publication 28*, pages 3–18, 1987.

J. A. Jackson and N. J. White. Normal faulting in the upper continental crust: observations from regions of active extension. *Journal of Structural Geology*, 1(36), 1989.

B. E. John and D. A. Foster. Structural and thermal constraints on the initiation angle of detachment faulting in the southern Basin and Range: The Chemehuevi Mountains case study. *Geological Society of America Bulletin*, 105(8):1091–1108, 1993. ISSN 00167606. doi: 10.1130/0016-7606(1993)105¡1091:SATCOT¿2.3.CO;2.

R. F. Livaccari, J. W. Geissman, and S. J. Reynolds. Large-magnitude extensional deformation in the South Mountains metamorphic core complex, Arizona: evaluation with paleomagnetism. *Geological Society of America Bulletin*, 107(8):877–894, aug 1995. ISSN 00167606. doi: 10.1130/0016-7606(1995)107¡0877:LMEDIT¿2.3.CO;2.

D. P. Maxbauer, J. M. Feinberg, and D. L. Fox. MAX UnMix: A web application for unmixing magnetic coercivity distributions. *Computers & Geosciences*, 95:140–145, oct 2016. ISSN 00983004. doi: 10.1016/j.cageo.2016.07.009.

M. W. McElhinny and P. L. McFadden. Palaeosecular variation over the past 5 Myr based on a new generalized database. *Geophysical Journal International*, 131(2):240–252, nov 1997. ISSN 0956540X. doi: 10.1111/j.1365-246X.1997.tb01219.x.

P. L. McFadden, R. T. Merrill, and M. W. McElhinny. Dipole/Quadrupole Family Modeling of Paleosecular Variation. Technical Report B10, 1988.

P. W. Monigle, J. Nabelek, J. Braunmiller, and N. S. Carpenter. Evidence for low-angle normal faulting in the Pumqu-Xianza Rift, Tibet. *Geophysical Journal International*, 190(3):1335–1340, 2012. ISSN 0956540X. doi: 10.1111/j.1365-246X.2012.05581.x.

S. J. Reynolds, M. Shafiqullah, P. E. Damon, and E. DeWitt. Early Miocene mylonitization and detachment faulting, South Mountains, central Arizona. *Geology*, 14(4):283, apr 1986. ISSN 0091-7613. doi: 10.1130/0091-7613(1986)14¡283:EMMADF¿2.0.CO;2.

R. J. Scott and G. S. Lister. Detachment faults: evidence for a low-angle origin. *Geology*, 20(9): 833–836, sep 1992. ISSN 00917613. doi: 10.1130/0091-7613(1992)020¡0833:DFEFAL¿2.3.CO;2.

R. H. Sibson. Generation of Pseudotachylyte by Ancient Seismic Faulting. *Geophysical Journal International*, 43(3):775–794, dec 1975. ISSN 0956-540X. doi: 10.1111/j.1365-246X.1975.tb06195.x.

D. M. Smith. *Pseudotachylytes of the South Mountains metamorphic core complex, AZ: A record of low-angle normal fault seismicity.* PhD thesis, University of Wisconsin - Madison, 2013.

J. E. Spencer. Role of tectonic denudation in warping and uplift of low-angle normal faults (USA). *Geology*, 12(2):95–98, 1984. ISSN 00917613. doi: 10.1130/0091-7613(1984)12¡95:ROTDIW¿2.0.CO;2.

L. Tauxe, R. Shaar, L. Jonestrask, N. L. Swanson-Hysell, R. Minnett, A. A. P. Koppers, C. G. Constable, N. Jarboe, K. Gaastra, and L. Fairchild. PmagPy: Software package for paleomagnetic data analysis and a bridge to the Magnetics Information Consortium (MagIC) Database. *Geochemistry, Geophysics, Geosystems*, 17(6):2450–2463, jun 2016. ISSN 15252027. doi: 10.1002/2016GC006307.

D. Wang and R. Van der Voo. The hysteresis properties of multidomain magnetite and titanomagnetite/titanomaghemite in mid-ocean ridge basalts. *Earth and Planetary Science Letters*, 220 (1-2):175–184, mar 2004. ISSN 0012821X. doi: 10.1016/S0012-821X(04)00052-4.

B. Wernicke. Cenozoic Extensional tectonics of the U.S. Cordillera. In *The Cordilleran Orogen: Conterminous U.S.*, chapter 12, pages 553–581. Geological Society of America, Boulder, CO, 1992.

B. Wernicke and G. J. Axen. On the role of isostasy in the evolution of normal fault systems. *Geology*, 16:848–851, 1988.

D. L. Whitney, C. Teyssier, P. Rey, and W. Roger Buck. Continental and oceanic core complexes. *Bulletin of the Geological Society of America*, 125(3-4):273–298, 2013. ISSN 00167606. doi: 10.1130/B30754.1.

S. Wills and W. R. Buck. Stress-field rotation and rooted detachment faults: A Coulomb failure analysis. *Journal of Geophysical Research*, 102(B9):20503–20514, sep 1997. ISSN 0148-0227. doi: 10.1029/97JB01512.

M. S. Zechmeister, E. C. Ferré, M. A. Cosca, and J. W. Geissman. Slow and fast deformation in the Dora Maira Massif, Italian Alps: Pseudotachylytes and inferences on exhumation history. 2007. doi: 10.1016/j.jsg.2007.03.009.